CANADIAN THESES

THÈSES CANADIENNES

NOTICE

The quality of this microfiche is heavily dependent upon the quality of the original thesis submitted for microfilming. Every effort has been made to ensure the highest quality of reproduction possible.

If pages are missing, contact the university which granted the degree.

Some pages may have indistinct print especially if the original pages were typed with a poor typewriter ribbon or if the university sent us an inferior photocopy.

Previously copyrighted materials (journal articles, published tests, etc.) are not filmed.

Reproduction in full or in part of this film is governed by the Canadian Copyright Act, R.S.C. 1970, c. C-30.

AVIS

La qualité de cette microfiche dépend grandement de la qualité de la thèse soumise au microfilmage. Nous avons tout fait pour assurer une qualité supérieure de reproduction.

S'il manque des pages, veuillez communiquer avec l'université qui a conféré le grade.

La qualité d'impression de certaines pages peut laisser à désirer, surtout si les pages originales ont été dactylographiées à l'aide d'un ruban usé ou si l'université nous a fait parvenir une photocopie de qualité inférieure.

Les documents qui font déjà l'objet d'un droit d'auteur (articles de revue, examens publiés, etc.) ne sont pas microfilmés.

La reproduction, même partielle, de ce microfilm est soumise à la Loi canadienne sur le droit d'auteur, SRC 1970, c. C-30.

THIS DISSERTATION HAS BEEN MICROFILMED EXACTLY AS RECEIVED

LA THÈSE A ÉTÉ MICROFILMÉE TELLE QUE NOUS L'AVONS REÇUE

THE UNIVERSITY OF ALBERTA

THE STUDY OF THE BOUNDARY LAYER FLOW OF AN ELECTRIC ARC

by

© STEPHEN SIU-KI AU

A THESIS

SUBMITTED TO THE FACULTY OF GRADUATE STUDIES AND RESEARCH

IN PARTIAL FULFILMENT OF THE REQUIREMENTS FOR THE DEGREE

OF DOCTOR OF PHILOSOPHY

DEPARTMENT OF ELECTRICAL ENGINEERING

EDMONTON, ALBERTA

FALL 1986

ISBN 0-315-32612-3

THE UNIVERSITY OF ALBERTA

RELEASE FORM

NAME OF AUTHOR STEPHEN SIU-KI AU

TITLE OF THESIS THE STUDY OF THE BOUNDARY LAYER FLOW OF AN ELECTRIC ARC

DEGREE FOR WHICH THESIS WAS PRESENTED DOCTOR OF PHILOSOPHY

YEAR THIS DEGREE GRANTED FALL 1986

Permission is hereby granted to THE UNIVERSITY OF ALBERTA LIBRARY to reproduce single copies of this thesis and to lend or sell such copies for private, scholarly or scientific research purposes only.

The author reserves other publication rights, and neither the thesis nor extensive extracts from it may be printed or otherwise reproduced without the author's written permission.

(SIGNED) .....

PERMANENT ADDRESS:

16, Bedwood Road, N.E.,

Calgary, Alberta, Canada,

T3K 2K4

DATED 26 th September, 1986

THE UNIVERSITY OF ALBERTA

FACULTY OF GRADUATE STUDIES AND RESEARCH

The undersigned certify that they have read, and recommend to the Faculty of Graduate Studies and Research, for acceptance, a thesis entitled The study of the boundary layer flow of an electric arc submitted by Stephen Siu-Ki Au in partial fulfilment of the requirements for the degree of Doctor of Philosophy.

Peter R Smy
.....
Supervisor

F.E. Kennedy
.....

.....

Adam Kowalski
.....

J.L. Lauzon
.....
External Examiner

Date 26th September, 1986

Dedication

To my wife,Cecilia

Abstract

The interaction of an electric arc flowing within channels of an arc chute installed in a cross-blast type air circuit breaker was investigated. Experimental studies of the thermal and electrical properties of such a layered arc were conducted by means of blasting an electric arc onto a ceramic flat plate, into a double plate channel or into a multiple array of plates within a shock tube.

Two dimensional boundary layer flow models incorporated with temperature scaling were developed for an arc flowing on : (1) a single plate and (2) a double plate system. The variation of electric field with current and the temperature profiles of the arc are predicted for both situations. Measurements of the field and current magnitudes were found in agreement with predicted values within a discrepancy of about 20% . The arc intensity profiles between two plates were found to match with the 8^{th} power of the predicted temperature profiles for a single plate. The spatial spread of the intensity profiles above a plate reveals that the arc thickness is within 2 to 3 mm at a downstream distance of 1.5 cm from the leading edge of the plate.

Acknowledgement

I would like to express my gratitude to Dr. Peter Smy who gave invaluable guidance and supervision throughout the project.

Many thanks to Doug Way-Nee for his technical assistance, discussions and instructions, especially, the advice on the use of densitometer.

I am also indebted to Dr. Jaime Santiago and Richard Haley for their invaluable technical discussions and advice.

Much appreciations are directed to Dr. Dennis Simeoni, Dr. Farouk Soliman, Sam Ghufran, Brian Stephen, Christ Way-Nee and Lin Duquette for their companionship.

Thanks are also directed to Terry Butler for his suggestions and assistance in using microcomputers.

I also thank the National Research Council of Canada (NSERC) for their financial assistance.

Finally, the excellent typing done by my sister, Pauline and my wife, Cecilia is deeply appreciated.

Table of Contents

List of Tables

List of Figures

List of Plates

1. Introduction

The escalating consumption of electrical energy in the past 50 years has imposed heavy dependence on power generation and transmission networks. Reliable operation of such systems becomes an indispensable factor in the provision of the necessary power. Any malfunctioning of the networks can cause disastrous power blackouts [1]. Protective devices thus act as an important element in insuring normal power transmission.

Circuit breakers [2] are essentially protective switches used to connect and disconnect various parts of the electric grids under hazardous situations. The presently used circuit breakers basically include the oil circuit breaker, the air circuit breaker, the sulfur hexafluoride circuit breaker and the vacuum circuit breaker. Detailed descriptions of these devices are given in Chapter 2.

All these circuit breakers serve a single purpose - the extinction of an electric arc. The switch basically consists of a pair of metal contacts which are in contact during normal power transmission. When a hazardous situation develops, the contact is opened. When the contact is just separated, a high voltage gradient is induced between the electrodes. The contact points are heated up and form a thin bridge of molten metal which eventually becomes so hot that

it vaporizes and an electrical breakdown results with the formation of an electric arc between the contacts. The physical nature of the electric arc has been studied by many researchers [3,4,5,6,7].

Since the arc is a column of hot and ionized gas, the quenching mechanisms are concerned with the processes of arc cooling and deionizing. Oil, air, sulphur hexafluoride and vacuum are used as quenching agents. Studies of the use of such media in various types of breakers can be found in some references [8,9]. Each agent has its own advantages and disadvantages; however, the most successful devices for interrupting the highest currents are those using air [1].

Air circuit breakers are generally of 2 types : magnetic air break circuit breakers which are limited to circuits of 15 KV or less and air blast circuit breakers. The first type [11,12,13] uses a magnetic field to force the electric arc into an arc chute where cooling and deionization take place. As the arc is driven into the chute, its length and resistance increase causing a steady increase in voltage drop across the arc. Eventually, the circuit imposed voltage across the contact is not high enough to support the arc voltage and the arc extinguishes. The second type includes an axial blast or a cross blast of air. In the axially blown type [14], the electric arc is

subjected to a strong flow of compressed air along its axis. The arc is interrupted by the process of convection. In the cross blast circuit breaker [15,16,17], the arc is forced by compressed air into an arc chute. Theories explaining the arc quenching mechanisms within the splitters were proposed by Prince [17] and Slepian [18]. According to Prince's 'displacement theory', the arc is cut into smaller sections upon entering the chute and the products are blown away further down the chute. The theory further predicts the recovery strength of the contact gap to be the product of the rate of fluid flow and the dielectric strength of the oncoming air displacing the arc. However, Slepian argued that the physical discontinuity of the arc at the front of the barriers violates well known hydrodynamic principles. Moreover, he suggested that the flow of high velocity air creates turbulence which causes more rapid mixing of highly ionized and unionized gases. Such mixing increases the diffusion rate by a few orders of magnitude and hence speeds up the dilution of ions into the bulk gas volume. Smy and Topham [19] explained the cooling effect by incorporating the hydrodynamic and thermal boundary layers formed around the leading edge of the plate into the theory. By using a moving cylindrical probe sweeping across a stationary arc, they were able to observe an increase in electric field due

to the cooling of the cylinder. Streak pictures indicate the cooling effect in a boundary layer at the probe surface. The work was further extended by using aerofoils with a circular leading edge and tapered trailing edge about 4 cm behind the leading edge [20]. They found that boundary layer cooling plays a significant role in the operations of the cross blast type circuit breakers. However, their experiments did not really simulate the actual arc motion in the cross blast circuit breakers.

The present work involves a more realistic and detailed investigation of a layered arc flowing on a flat surface. Instead of using a stationary arc and a moving probe system, a combination of stationary probes and a moving arc is used. A system is adopted in which a stationary arc is held against a flat surface by gas flow. Such an arrangement will closely resemble the situation in which the arc is swept into an arc chute in a cross blast circuit breaker. The physical and electrical properties of the arc are more easily monitored and understood in such a configuration. The motivation for this study is the hope that it will provide information to help determine the appropriate values of the various breaker design parameters such as separation of arc barriers, number of arc barriers, air pressure, air volume, etc. All these parameters may be influential in determining

the breaking capability of the circuit breaker.

Situations of the arc flowing : (1) on a single flat surface, (2) within a pair of flat surfaces of given separation, (3) against a stack of plates at fixed gap widths are briefly analyzed. The electrical and physical characteristics are measured and compared with the calculations. Reasonable agreement between theory and experiment is found.

A brief review of the four types of circuit breakers is given in Chapter Two. The different types of instruments used throughout the measurement are described in Chapter Three. The theory of an arc flowing along a single flat plate is analyzed in Chapter Four. Experimental results for an arc flowing along a short plate and a long plate are also given and compared with the theory. Chapter Five accounts for an arc flowing between two flat plates. Different arc configurations are analyzed separately. The physical profile of the arc was found experimentally and compared with the calculations. Chapter Six consists of an overall discussion and a general account of what might be done in future investigations.

2. Review of circuit breakers

2.1 Outline

In power transmission networks, circuit breakers serve as indispensable devices for protecting the system from electrical and mechanical hazards. The circuit breakers will disconnect malfunctioning parts from the system configuration whenever failures occur. Different types of circuit breakers are designed with different current interrupting capacities to fit various circuit ratings. Oil, air, sulphur hexafluoride and vacuum are used as breaking media. A brief discussion of the various types of breakers using the aforementioned media as quenching agents now follows.

2.2 Oil circuit breaker

Mineral oil is used in the oil circuit breaker as an arc suppressing medium. Current carrying contacts are submerged in a tank of oil. Upon contact separation or closure, an arc is drawn between them. The heat generated from the arc vaporizes the surrounding oil and dissociates it into carbon and gaseous hydrogen [3]. Since hydrogen has a high thermal conductivity, it conducts the heat of the arc away very quickly with the result that the arc is extinguished in a short time. Explosion hazards might occur

if the hot hydrogen gas is exposed to air, and so the arcing contacts are immersed deep enough in oil to prevent any hot hydrogen gas coming in contact with air.

In some oil breakers, a rigid insulating chamber encloses the arcing contacts to improve the arc interruption efficiency since higher gas pressure is built up as the arcing contacts separate. When the contact rod is pulled away from the chamber outlet, hydrogen gas escapes at high speed and the arc is thus subjected to a strong flow of gas and a more severe quenching results.

As a result of oil dissociation, carbon deposits are formed and reduce the oil dielectric strength. The interrupting power of the breaker hence deteriorates with the age of the breaker. Constant cleaning of the oil is necessary for proper breaker performance. Moreover, potential risks of oil, fire and oil explosions contribute a hazardous factor to this type of circuit breaker.

2.3 Air circuit breaker

Circuit breakers using air as a quenching medium were developed about 1940. Such breakers are clean, easily maintained and free from oil, fire and oil explosion hazards. For low and medium breaking voltage ratings, air breakers are of the cross blast type. For high voltage

ratings, axial blast air breakers are usually used [21]. In the cross blast type circuit breaker, an arc chute is built in for arc cooling purposes. The chute is comprised of a stack of metal plates insulated with ceramic on the surface. The plates are separated at a fixed distance. Upon contact separation, an arc is formed and is driven into the arc chute either by an external magnetic field [11] or by compressed air. The arc is stretched, cooled and eventually extinguished among the gaps [22]. In the axial blast type, compressed air is released through a nozzle and its flow is directed axially onto the arc upon contact separation. The arc is thus drastically cooled and quenched.

Although such breakers have certain advantages over the oil circuit breakers, the complexity of the breaker system, the large volume of compressed air consumed and high noise level detract from its usefulness.

2.4 Sulphur hexafluoride circuit breaker

Circuit breakers using sulphur hexafluoride gas have been developed over the last 30 years. They are used in networks requiring high voltage ratings [8,9] of the network electrical equipment. Sulphur hexafluoride has a low thermal conductivity but high electrical conductivity at high temperature. The opposite is true at low temperature. Arcs

with relatively small radius are favorably formed within this gas. The heat of the arc core cannot be conducted away by the surrounding gas because of the low thermal conductivity of the gas. As a result, the region close to the arc core will remain at a relatively low temperature, leading to a low electrical conductivity. The arc is thus confined to a thin core having a high temperature and is surrounded by a non-conducting layer. The thermal time constant[1] which is proportional to the arc radius, becomes very small. A small thermal time constant allows the initial temperature of the arc to decrease rapidly. At temperature below 3000°K, the molecules of sulphur hexafluoride (SF_6) and its decompositon products (SF_5, SF_4, SF_2, etc.) would strongly absorb the electrons of the decaying arc and create negative ions. It is believed that these ions have low mobilities, causing a rapid increase in the discharge resistance [10].

In spite of the gas having ideal arc quenching properties, its decomposed products, in the presence of moisture, erode the various components of the circuit breaker and also form insulating materials with vaporised metals. Such corrosive characteristics present problems in

---

[1]Thermal time constant of an arc is defined as the time required to reduce the arc conductance by a factor 1/e due to temperature decay. It depends on the ratio of A/D, where A is the cross sectional area of arc. D is the diffusion coefficient or thermal conductivity.

the durability of this type of breaker.

2.5 Vacuum circuit breaker

The vacuum circuit breaker has been developed in recent years [23]. The latest applications are confined to over-voltages less than or equal to about 40 kV because of various design constraints. In this type of interrupter, the metal contact is shielded within a vapor condensation shield under high vacuum. The contact can be opened by withdrawing the bellows contact from the stationary contact. Material for the metal contact is chosen to have high electrical conductivity and low weld strength. Upon separation, the high electric field between the contact gap will create hot spots on the surface of the metal. Metal is vaporised from the surface and condenses on the shield. This type of breaker has the advantage of minimum maintenance, compact size and is noise free except for the noise from the operating mechanisms. Furthermore, the maximum contact stroke need only be in the range of several millimeters to several centimeters.

6 Summary

Different types of circuit breakers have been briefly explained. Each type has its particular arc cooling features. However, the mechanism of arc quenching is still a challenging problem. An understanding of arc cooling mechanisms is a major part of the study of circuit breakers.

3. Instrumentation

3.1 Outline

An arc being discharged in the presence of a fast flowing gas generated in a shock tube was studied. The means for generating an arc and the appropriate gas flow as well as the various diagnostic techniques used throughout the investigation are described.

3.2 Shock tube

The flow of gas was generated within a shock tube as shown in Figure 3.1. The tube included a driver section, a driven section and a dump tank. The overall tube length was approximately two meters. Mylar sheets of thickness ≈25 μm and ≈50 μm were used as diaphragms for creating the desired shock speeds. Air was usually used as a driver gas. The pressure in the driver section was kept at 340 kPa absolute (3 atmosphere absolute) for the thinner Mylar sheet and 600 kPa absolute (6 atmosphere absolute) for the thicker one. The pressure in the driven section was kept at 100 kPa absolute (atmospheric) or 10 kPa absolute (1/10 atmospheric pressure). A test compartment followed by a dump tank was connected to the end of the driven section. A pressure transducer was mounted on the driven section close to the Mylar diaphragm for triggering purposes. Air release valves

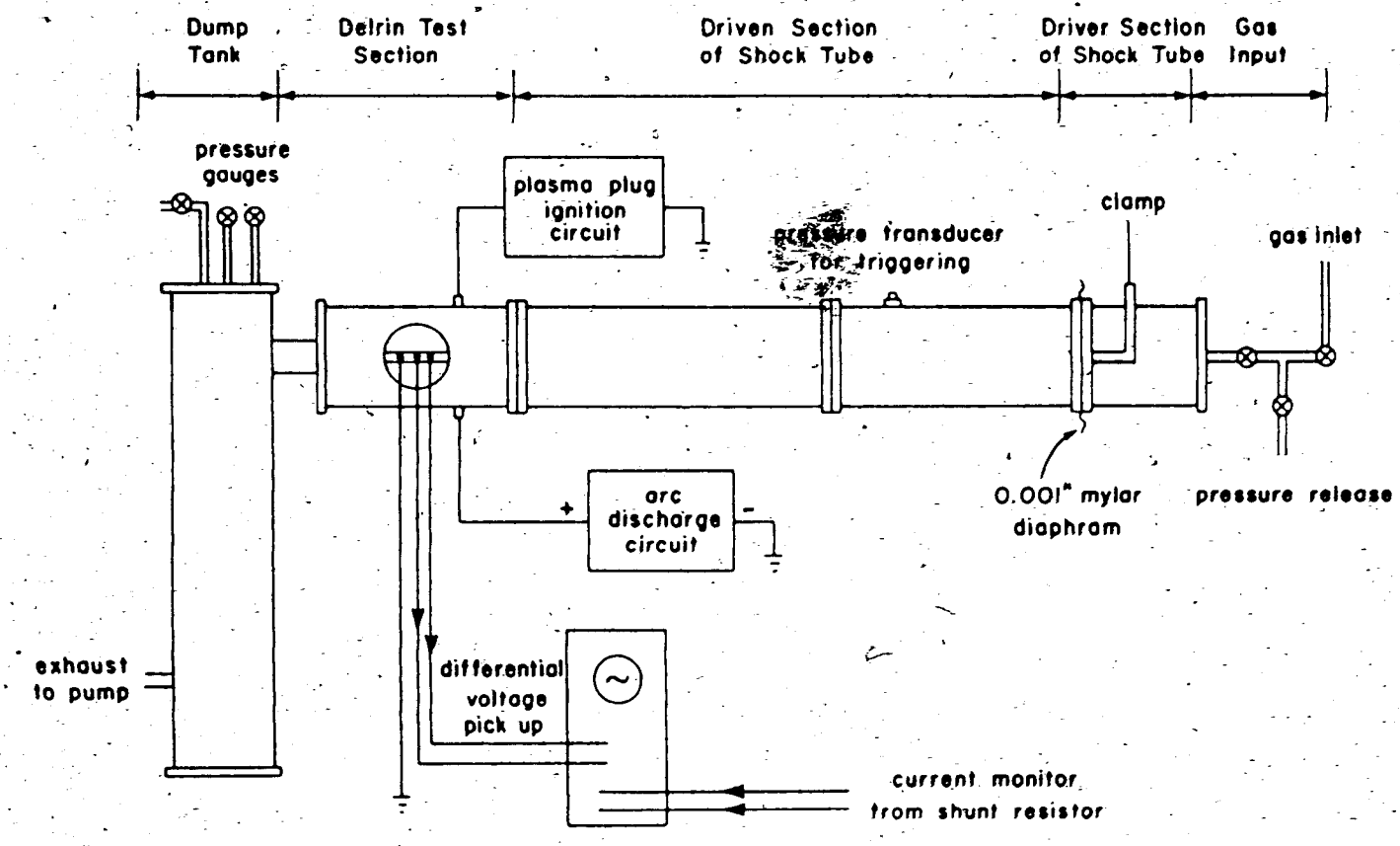

Figure 3.1 The schematic of the shock tube.

were connected to both driver and driven sections.

3.3 Test section

The testing section was a rectangular air-tight Delrin cavity, as shown in Figure 3.2(a), in which the interaction between the arc and gas flow takes place. A wedge cut from ceramic stove top material which was 0.4 cm thick was mounted within the cavity. The wedge angle is within 20° to the flat surface. Brass strips at a separation of 1 cm were set flush with the top surface of the ceramic. Two 5 cm diameter and 1.25 cm thick glass windows were installed on opposite sides of the cavity to allow optical observation of the arc. Two axially aligned stainless steel cylindrical electrodes were mounted at a distance of 1 cm (centre of electrode to leading edge) from the leading edge of the wedge. Appropriate dimensions are given in Figure 3.2(b). A plasma plug[2] was embedded in one of the metallic electrodes for initiating the discharge. The tips of the electrodes were made with tungsten alloy which can withstand arc corrosions better than other material.

---

[2]A plasma plug is a modified version of a standard surface discharge igniter. It is made of a 1/16" diameter tungsten rod surrounded by a ceramic pipe which, in turn is surrounded by a steel pipe. One end of the pipe is covered with a circular steel disc with a hole punched at the centre of the disc. The rod is positioned at a certain distance from the disc (Figure 3.2(c)). A plasma plume is created through the hole of the disc by charging the rod to a high voltage and grounding the outer steel cyclinder. Further details can be found in the work by Simeoni. [24].

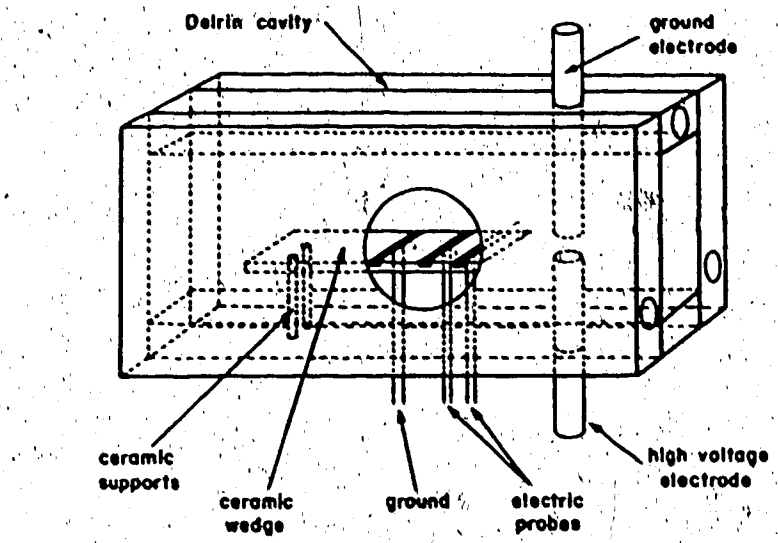

(a)

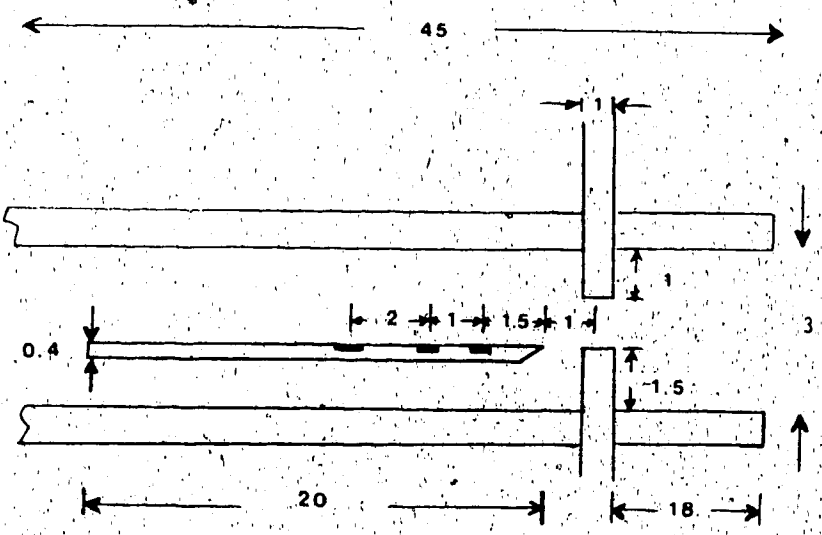

Scales are in cm.

Cavity size :
3 cm x 6 cm

(b)

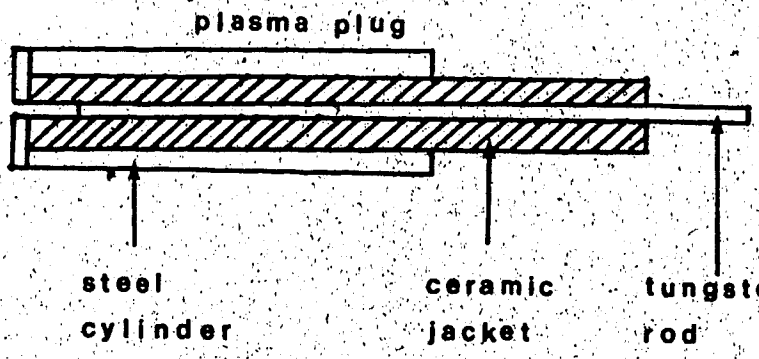

(c)

Figure 3.2 Set-up of the test section.

3.4 Power supply and plasma plug ignition circuit

The power supply for the arc consisted of a series RLC circuit which included three 240 μF, 5 kV capacitors connected in parallel as shown in Figure 3.3. A copper coil with an inductance of about 7 mH was connected in series with the capacitor. A shunt resistor of 1/6 Ω was used as a current monitor. Resistances were added to provide the appropriate current. A plasma plug ignition circuit, shown in Figure 3.4, was used to initiate the main discharge. Throughout the experiments, the capacitors were charged between 600 V and 2 kV.

3.5 Measuring instruments

Major diagnostic equipment for the arc included the Tektronix 556 dual trace oscilloscope and the P6015 HV probe, a TRW model 1-D streak camera, a Kodak Spin Physics SP 2000 Motion Analysis System and a model MK III C auto-recording microdensitometer manufactured by Joyce and Loebl Co. Ltd.

3.5.1 Streak Camera

The streak camera is a high speed electronic camera which uses an image converter tube. Incident light is received at the photocathode end of the tube. The cathode is optically excited and emits a beam of electrons. This

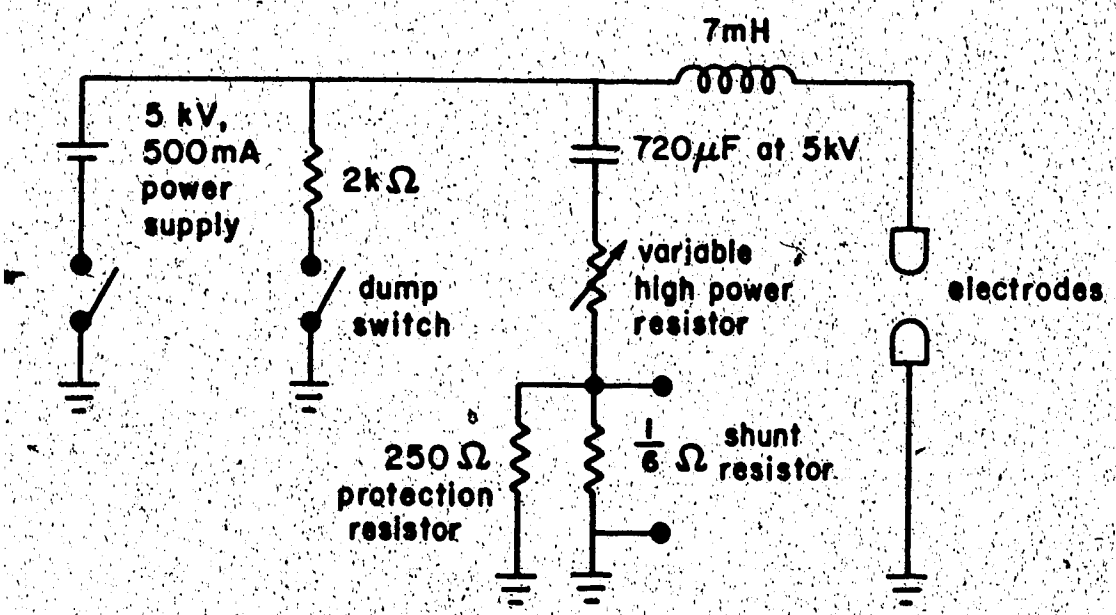

Figure 3.3 RLC discharging circuit diagram.

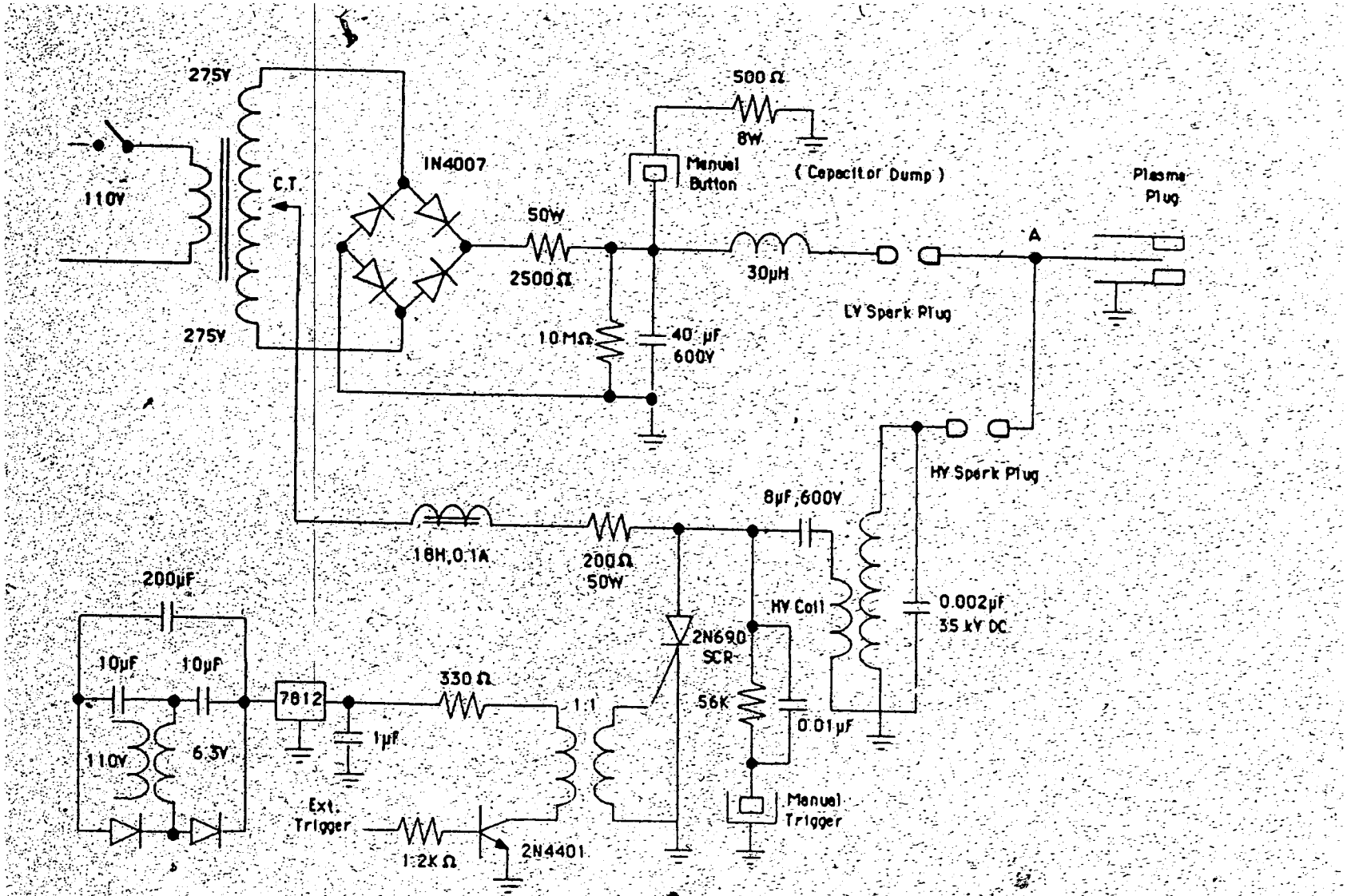

Figure 3.4 Plasma plug ignition circuit.

electron beam, being controlled by a sweeping potential, streaks across a fluorescent screen on which a trace of the illuminating object is displayed. If the object has a time varying brightness, the trace on the screen will reveal such changes. The camera is used to record the light intensity of particular arc portions. A streaking period of 50 μs was chosen for the observation of temporal changes of the physical dimensions of the arc.

3.5.2 Spin Physics SP 2000 Motion Analysis System

The SP 2000 Motion Analysis System is a high speed video camera which is capable of storing 2000 frames of data per second [25]. It includes a camera and a high speed recording unit.

The camera consists of a photocapacitive array sensor which has light gathering cells, called pixels, arranged in a 238 x 192 array. The 192 rows of cells are divided into six blocks of 32 rows each. The sensor is scanned one block at a time producing 32 channels of signals which are sent to the recording unit. When the six blocks of cells are completely scanned, a frame of data will be produced. Such block scanning can achieve a recording rate of 2000 frames of data per second.

The recording unit consists of a high speed digital to analog converter and an analog tape recorder. Scanned signals are modulated into video signals so that they can be displayed on any standard NTSC[1] monitor. Recorded video signals can be played back at a speed of one, two, three, four or sixty frames per second. Although the data transfer rate is limited to a maximum of 2000 frames per second, sensor scanning rate can be stepped up to a maximum of 12,000 pictures per second. For each scanning of the six blocks of pixels, only a single block of data will be recorded and stored in 1/6 of a frame. To complete an entire frame of data, six passes of scanning will have to be done. As a result, one frame will contain six pictures of the event. At a framing rate of 2000 frames per second, 12,000 pictures of an event can be recorded in 1 second.

3.5.3 Auto-recording microdensitometer

The operating principle of the microdensitometer is based on a true double-beam light system, in which, two beams from a single light source are switched alternately to a single photomultiplier. If the intensities of the two beams are different, the photomultiplier will produce a signal which causes a servo motor to move an optical attenuator so as to nullify the intensity difference. The

---

[1] National Television System Committee.

position of the attenuator is made to record the density at any particular part of the specimen which may be film, plate or other transparency. The instrument records density directly and linearly within the range of densities specified. A selection of grey wedges provides a range of density scales to be used for recording.

3.5.4 P6015 High Voltage Probe

The P6015 HV probe is a 1000X attenuator probe. It has an input resistance of 100 MΩ and capacitance of about 3 pf. A compensating box is associated with the probe for compensating any excessive impedances in the circuit which might distort the input signals.

4. Modelling and Experiments of arc flowing on a flat plate

4.1 Outline

A layered electric arc held against the surface of a flat plate by gas flow was analyzed theoretically. The energy balance between heat conduction, convection and joule heating was solved to obtain temperature profiles through the arc and the electric field-current characteristics of the system. These theoretical results are compared with measured values obtained by means of blasting an electric arc with a strong gas flow generated in a shock tube.

4.2 Introduction

In air blast circuit breakers, the arc drawn between contact gaps is driven by gas into an arc chute which is a stack of plates separated at a distance from each other. Cooling action takes place between the gaps. The arc extends over the surface of the chute plates as it flows between the plate channels. Conduction takes place between the 'sheet' of arc and the plate surface, while convection occurs between the cold gas and the arc. Radiation is neglected in this case as long as the arc temperature is below 12,000°K [26].

The motion of the arc is described by the 2-dimensional Prandtl boundary layer theory for a flat plate with the

inclusion of temperature variation. The temperature profile through the arc is solved with the combination of the modified Prandtl boundary layer theory and the heat flow equation for convection and conduction. The electric field-current characteristic of the system is then obtained from the integration of the current density throughout the arc.

4.3 Theory

4.3.1 Prandtl boundary layer theory over a flat plate

For boundary layer flow along a flat surface, the steady, 2-dimensional Prandtl boundary layer equations are [27]

$$u\frac{\partial u}{\partial x} + v\frac{\partial u}{\partial y} = \nu\frac{\partial^2 u}{\partial y^2} \tag{4.1}$$

and

$$\frac{\partial u}{\partial x} + \frac{\partial v}{\partial y} = 0 \tag{4.2}$$

with the boundary conditions that for $y = 0$, $u = 0$, $v = 0$, and for $y \to \infty$, $u \to U_0$, $v \to 0$. The x axis is parallel to the surface of the plate and the y-axis is perpendicular to the plate. Both axes are perpendicular to the front edge of the

plate (Figure 4.1), u and v are the components of the flow velocity in the x and y directions. Introducing a parameter

$$\eta = y\left[\frac{U_0}{\nu x}\right]^{1/2}$$

and a stream function, $\left[\nu x U_0 f(\eta)\right]^{1/2}$, both velocity components are found to be related as

$$\frac{u}{U_0} = f' \tag{4.3}$$

and

$$\frac{v}{U_0} = \frac{1}{2}(\eta f' - f)\left[\frac{\nu}{U_0 x}\right]^{1/2} \tag{4.4}$$

By substituting Equations 4.3 and 4.4, into Equations 4.1 and 4.2 the equations can be reduced into an ordinary differential equation

$$ff'' + 2f''' = 0 \tag{4.5}$$

subjected to the boundary conditions $\eta = 0$, $f = 0$, $f' = 0$, and $\eta \to \infty$, $f' = 1$. Solution of Equation 4.5 was obtained by Blasius [28]. Values of f, f', f'' are plotted in Figure 4.2 for illustration.

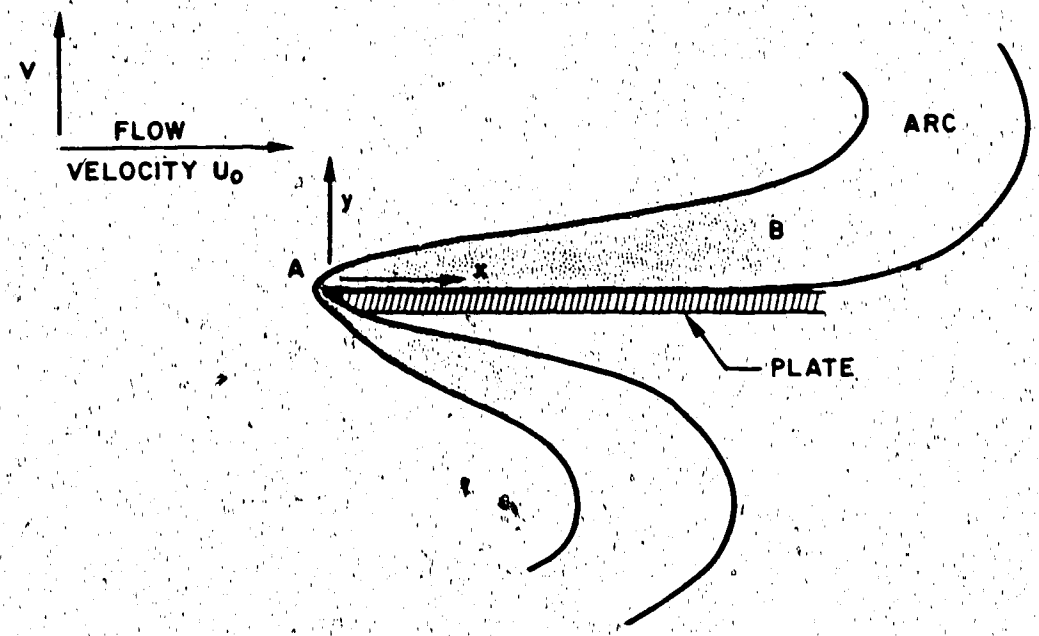

Figure 4.1 Arc flow on a wedge surface.

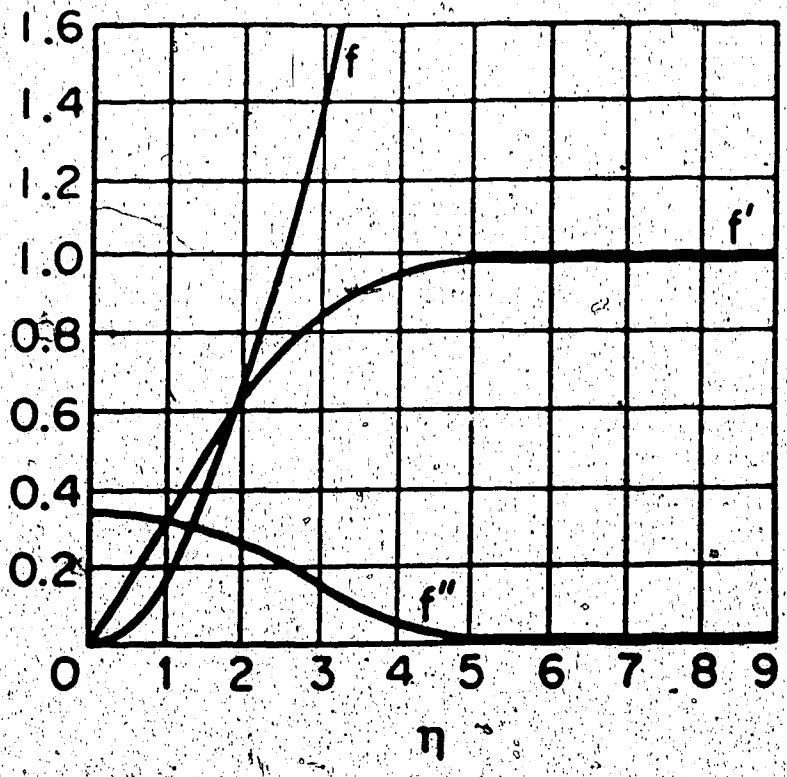

Figure 4.2 Values of f, f', f''

Variation of temperature throughout the flowing gas is not considered in previous summarized theory. In the present arc flow situation, the temperatures of the arc and the cold gas are very different. Such temperature variation results in substantial density and viscosity changes. Temperature variations of viscosity, thermal conductivity, electrical conductivity and specific heat of atmospheric pressure nitrogen are shown in Figure 4.3.

Simple power law approximations are used to describe the relations for viscosity, density, specific heat, thermal conductivity and electrical conductivity. The boundary layer equation can then be solved for a single solution which is readily transferable to other gases, using different constants of proportionality for the various parameters. In terms of the electric field versus current characteristics, it is the conduction of current across the total cross-section of the arc that is the issue. For this reason, the concept of 'smoothing' the temperature profiles is expected to give reasonable accuracy. In confirmation, it is found that the results are indeed remarkably insensitive to averaging. Thus, in an extreme example, it is found that the use of a constant value of c_p gives more or less identical results to those obtained with the much more realistic

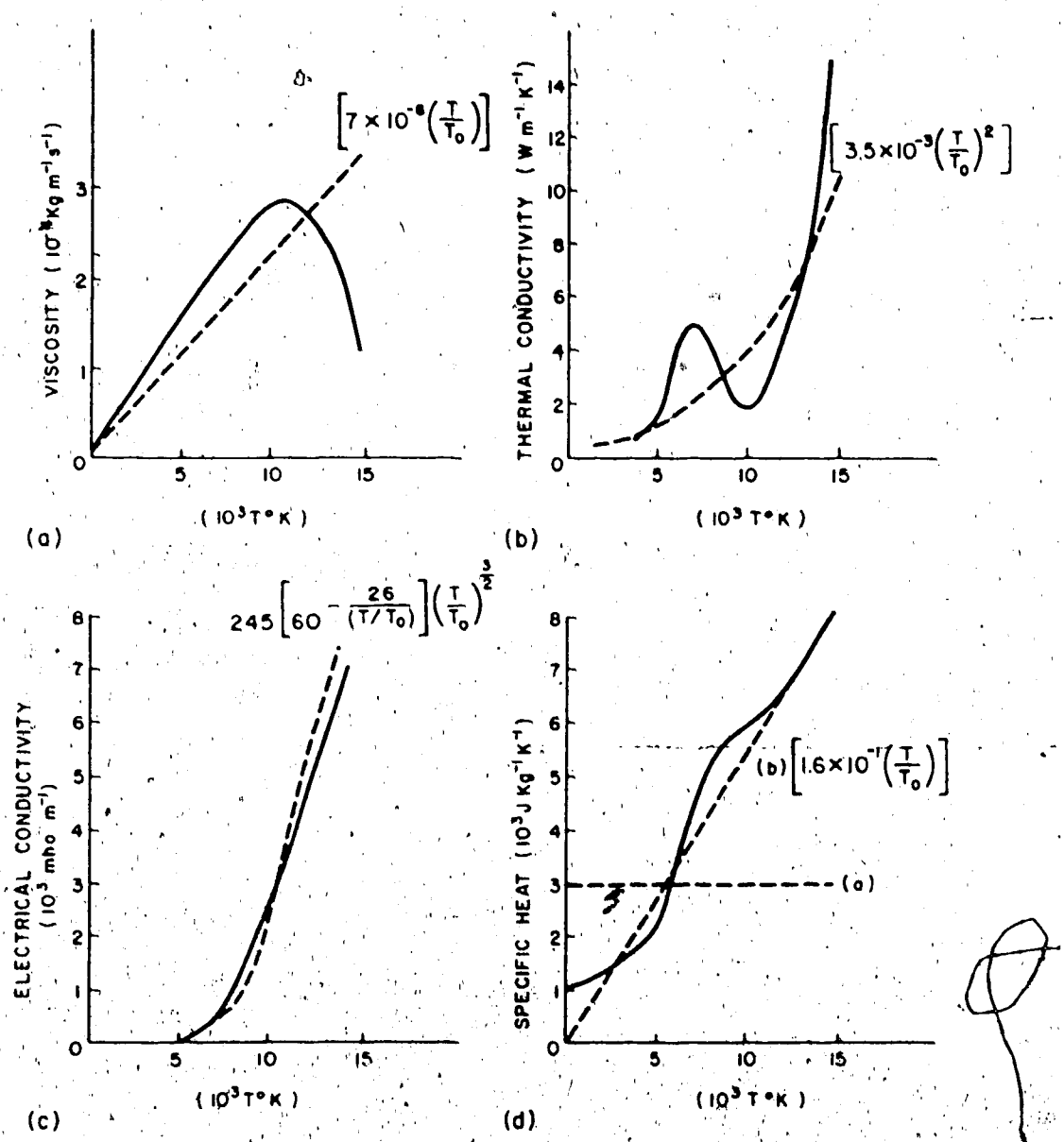

Figure 4.3 Variations of transport coefficients with temperature [27].

Since in a laminar boundary layer, the pressure perpendicular to the flow is constant, then for a given value of x, the density varies as temperature:

$$\rho = \rho_0 (\frac{T_0}{T}) \tag{4.6}$$

The kinematic viscosity ($\nu = \frac{\mu}{\rho}$) varies as the square of the temperature

$$\nu = \nu_0 (\frac{T}{T_0})^2 \tag{4.7}$$

where ρ_0 and ν_0 are the density and kinematic viscosity at $T = T_0 = 300°K$. Transforming variables:

$$dy = \frac{T}{T_0} dy_0$$

that is,

$$y = \int_{y_0=0}^{y_0} (\frac{T}{T_0}) dy_0 \tag{4.8}$$

$$v = \frac{T}{T_0} v_0 \tag{4.9}$$

reduces Equations 4.1 and 4.2 to

and

$$\frac{\partial u}{\partial x} + \frac{\partial v_0}{\partial y_0} = 0 \qquad (4.11)$$

Such a transformation, the so called Illingworth-Stewartson transformation [29], allows the original Blasius calculations for the boundary layer profile to be utilized in the determination of the boundary layer profile in the presence of temperature and compressibility effects. It is apparent in Equation 4.8 that the adjacent streamlines, separated at room temperature by dy_0, will move apart to a new separation dy because of thermal expansion. With ν scaling as T^2, it is evident that, with the mass flow between streamlines remaining unchanged, the shear force between these lines will also remain unchanged.

The temperature field is determined by the equation for conducted and convected heat flows, namely,

$$\rho c_p (u\frac{\partial T}{\partial x} + v\frac{\partial T}{\partial y}) = \frac{\partial}{\partial y}(K\frac{\partial T}{\partial y}) + \rho\nu(\frac{\partial u}{\partial y})^2 \qquad (4.12)$$

Compared to arc heating, viscous and stagnation heating effects will be negligible at subsonic or near-sonic velocities. A joule heating term, σE^2, is substituted for the last viscous term in Equation 4.12. Total heat loss of

ablation material from the flat plate has been ignored. The effects of ablation may be estimated following the procedure of Niemeyer [30]. The critical current densities when material loss starts to dominate the total heat losses are $\simeq 2 \times 10^6$ A/m^2 and 2×10^7 A/m^2 for an organic polymer and ceramic flat plate, respectively. For boundary layers of about 1 mm thick, these critical current densities correspond to 2×10^3 A/m and 2×10^4 A/m. Radiation losses are neglected as long as arc temperature remains below 12,000°K [26].

With K being described by

$$K = K_0\left[\frac{T}{T_0}\right]^2 \tag{4.13}$$

and σ fitting reasonably closely the following expression:

$$\sigma = \sigma_0\left[\frac{T}{T_0}\right]^{3/2} 60^{-26/(T/T_0)} \tag{4.14}$$

where $\sigma_0 = 245\ \Omega^{-1}m^{-1}$, Equation 4.12 becomes,

$$\rho c_p\left[u\frac{\partial T}{\partial x} + v\frac{\partial T}{\partial y}\right] = \frac{\partial}{\partial y}\left[K_0\left(\frac{T}{T_0}\right)^2\frac{\partial T}{\partial y}\right] + \sigma_0 E^2\left[\frac{T}{T_0}\right]^{3/2} 60^{-26/(T/T_0)} \tag{4.15}$$

with c_p being initially considered to vary as

$$c_p = c_{p0}\left[\frac{T}{T_0}\right]$$

$$\phi = \left[\frac{T}{T_0}\right]^2, \quad \eta = y_0\left[\frac{U_0}{\nu_0 x}\right]^{1/2} \tag{4.16}$$

and retaining Equation 4.3 and 4.4 for u and v, since they are unaltered by the transformation, we obtain

$$\frac{d^2\phi}{d\eta^2} = -\frac{\nu_0 C_{p0}\rho_0}{2K_0} f(\eta)\frac{d\phi}{d\eta} - \frac{2\sigma_0\nu_0\phi^{5/4}}{U_0 K_0 T_0}(E^2 x)60^{-26/(T/T_0)} \tag{4.17}$$

The term $\frac{\nu_0 C_{p0}\rho_0}{K_0}$ is the Prandtl number (P) evaluated for the bulk gas. Inserting values for $K_0 = 3.5 \times 10^{-3}\ Wm^{-1}K^{-1}$, $\mu_0 = \nu_0\rho_0 = 7 \times 10^{-6}\ kgs^{-1}m^{-1}$, $c_{p0} = 160\ Jkg^{-1}K^{-1}$, $\sigma_0 = 245\ \Omega^{-1}m^{-1}$, we obtained $P \simeq 0.3$. Rewriting Equation 4.17 with the constant $A = \frac{2\sigma_0\nu_0 E^2 x}{U_0 K_0 T_0}$

$$\frac{d^2\phi}{d\eta^2} = -\frac{P}{2} f(\eta)\frac{d\phi}{d\eta} - A\,\phi^{5/4}\,60^{-26/\sqrt{\phi}} \tag{4.18}$$

The boundary condition appropriate to this equation is that $\eta \to \infty$, $\phi \to 1$ and $\eta \to 0$, $\phi \to 1$. The factor E^2x in the constant A is treated as a constant. In fact, the electric field E along the plate surface is independent of η under steady state situation. Otherwise, the electric field gradient in the y direction, $\frac{\partial E}{\partial y}$ will generate a time varying magnetic field in a direction perpendicullar to both the gas

flow and the current flow. This boundary value equation is solved numerically [27] for various values of A. The results are shown in Figure 4.4 as profiles of normalized temperature ($\frac{T}{T_0} = \phi^{1/2}$) versus distance η profiles for $A = 1 \rightarrow 10^4$. Also shown in Figure 4.4 is the profile calculated for the condition $A = 1$ with $c_p = 3 \times 10^3$ $JKg^{-1}K^{-1}$. An order of magnitude variation in pressure compresses or expands the arc by less than a factor of two. The current per unit width parallel to the surface is

$$I = \int_{y=0}^{y=\infty} \sigma E \, dy \qquad (4.19)$$

which becomes

$$I = \left[\frac{K_0 \sigma_0 T_0 A}{2}\right]^{1/2} \int_{\eta=0}^{\eta=\infty} \phi^{5/4} \, 60^{-26/\sqrt{\phi}} \, d\eta \qquad (4.20)$$

The criterion that, for a given situation, I should remain constant and independent of x is clearly satisfied by the condition that A remains constant. Thus, the similarity approach in which a given value of A remains applicable throughout the arc is self consistent.

By integrating the temperature profiles of Figure 4.4 appropriately, we obtain a nondimensionalised electric field versus current characteristic (Figure 4.5). Also shown in Figure 4.5 (minor axes) are the values of current and electric field to be expected for a flow speed of 200 m/s

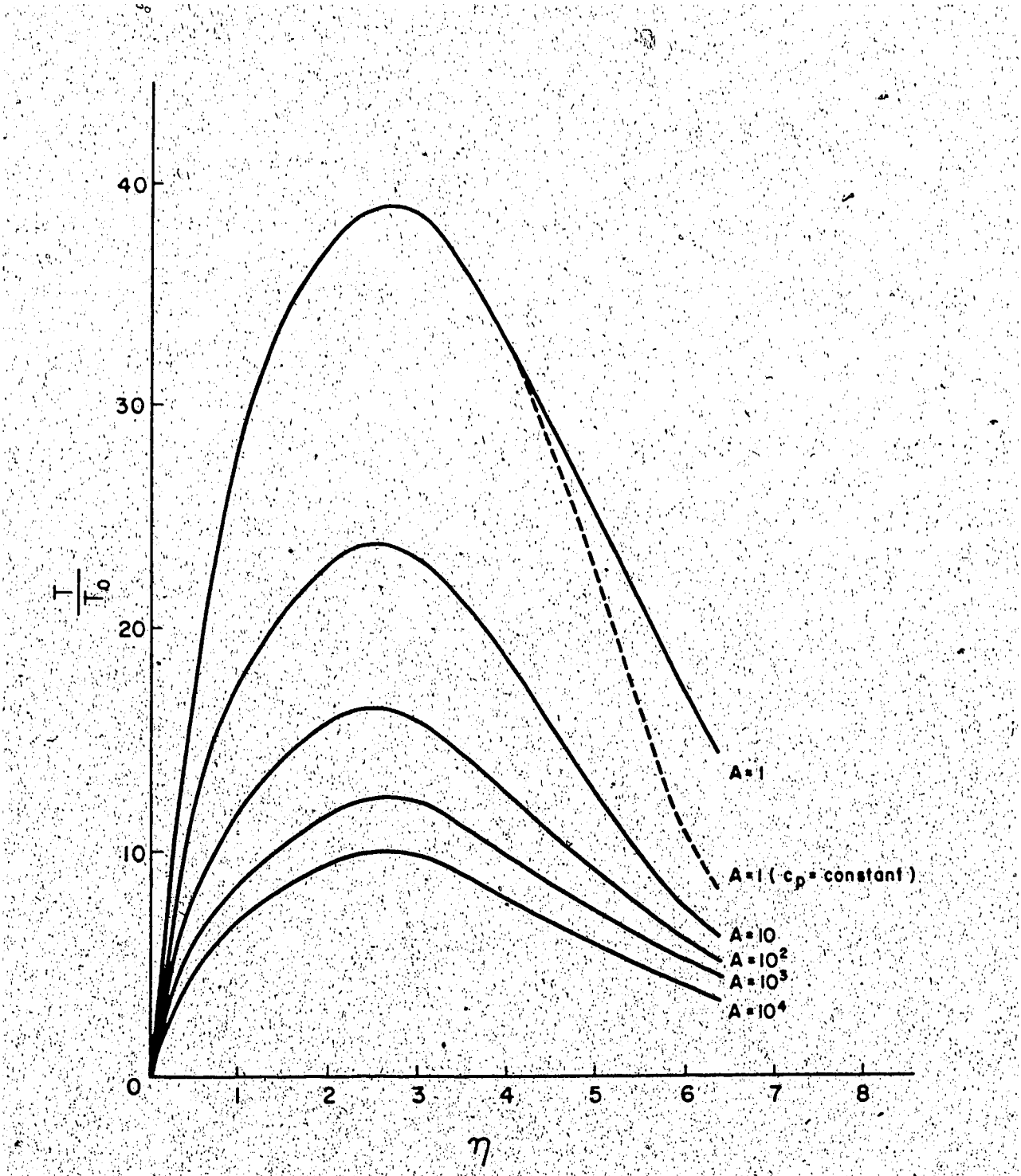

Figure 4.4 Normalized temperature profile above the plate surface.

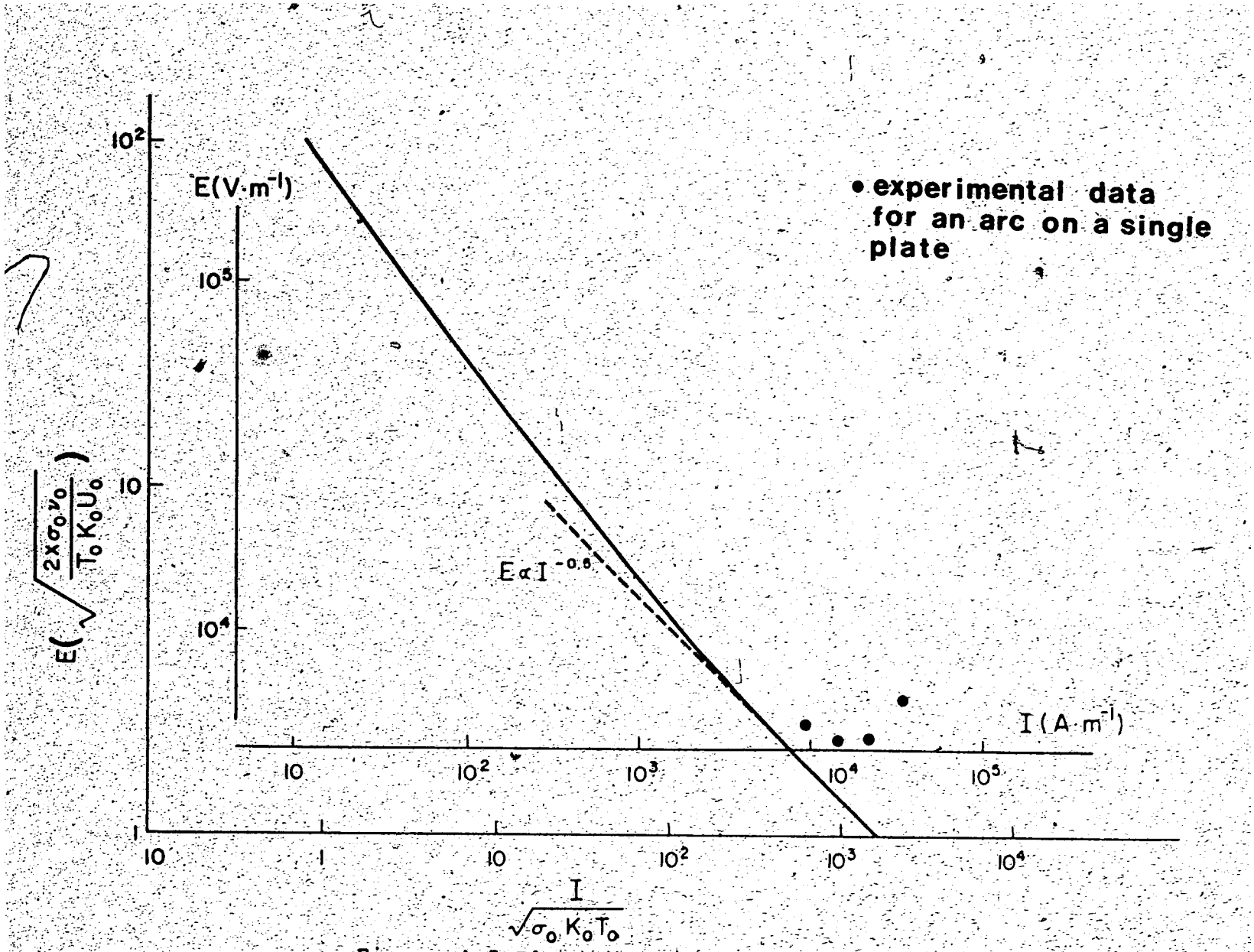

Figure 4.5 Electric field vs current.

and at a distance of 1 cm from the leading edge. It is noteworthy that the characteristic closely approximates to the electric field $\propto$ (current)$^{-0.5}$ behaviour observed in stationary arcs and in other convective arcs [27].

In terms of experimental verification of these calculations, a readily measurable parameter (in addition to electric field) is arc thickness. The profiles shown in Figure 4.4 are expressed in terms of the temperature transformed distance y_0 (via the quantity η). If the actual distance y is considered, the appropriate dimensionless quantity

$$\eta_A = y\left[\frac{U_0}{\nu_0 x}\right]^{1/2}$$

becomes:

$$\eta_A = \int \frac{T}{T_0}\, d\eta = \frac{T_{max}}{T_0} \int_{\eta=0}^{\eta=\infty} \frac{T}{T_{max}}\, d\eta \qquad (4.21)$$

where for each temperature profile (Figure 4.4) $\eta \approx 2$ when $T = T_{max}$. The above integral, carried out using values of T_{max} (Figure 4.6) taken from Figure 4.4, is found to be more or less independent of A and so yields a 'universal' temperature profile $(\frac{T}{T_{max}})$ versus $\eta_A(\frac{T_0}{T_{max}})$ for all values of A. The result is shown in Figure 4.7.

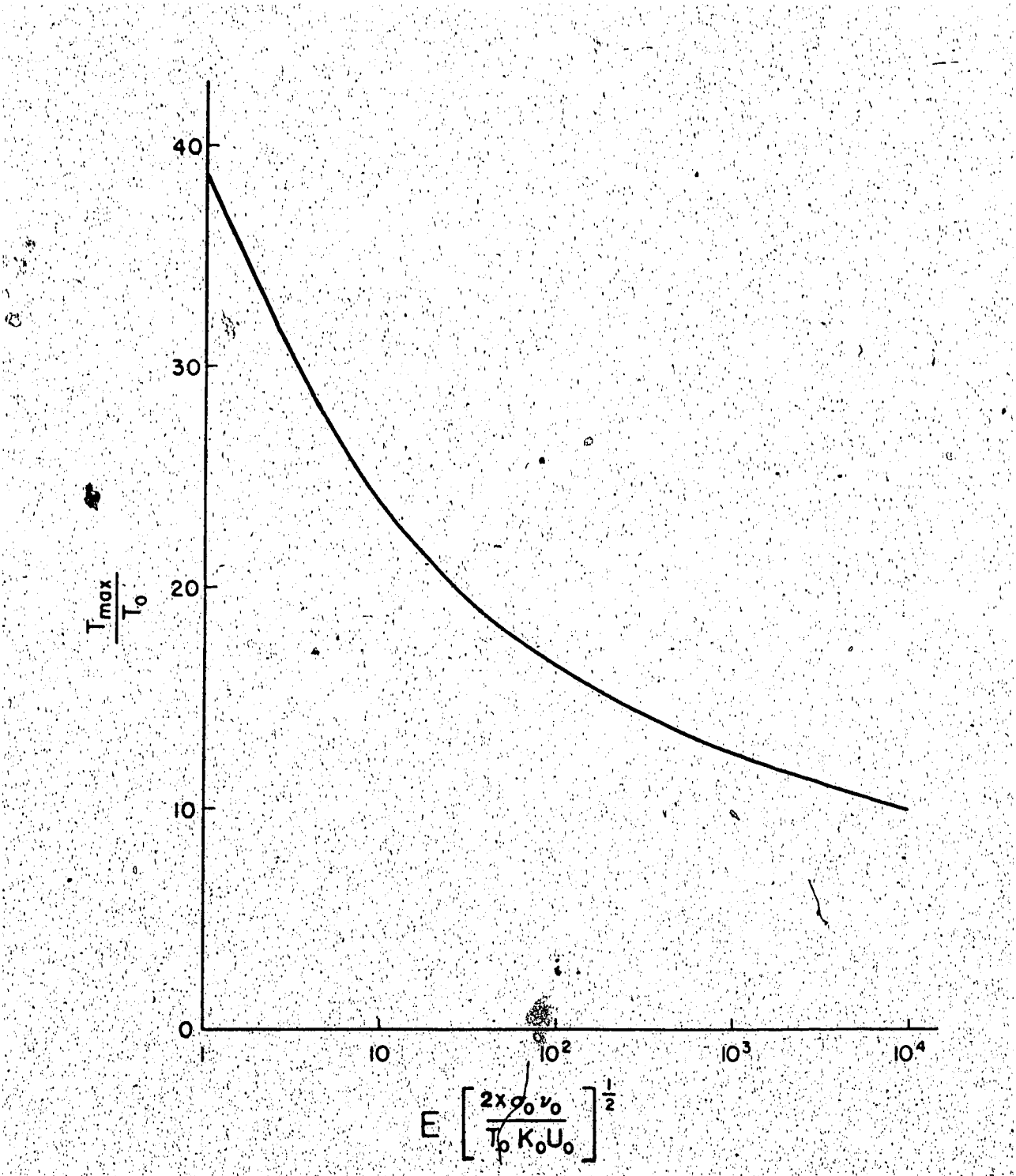

Figure 4.6 Normalized maximum temperature vs normalized electric field.

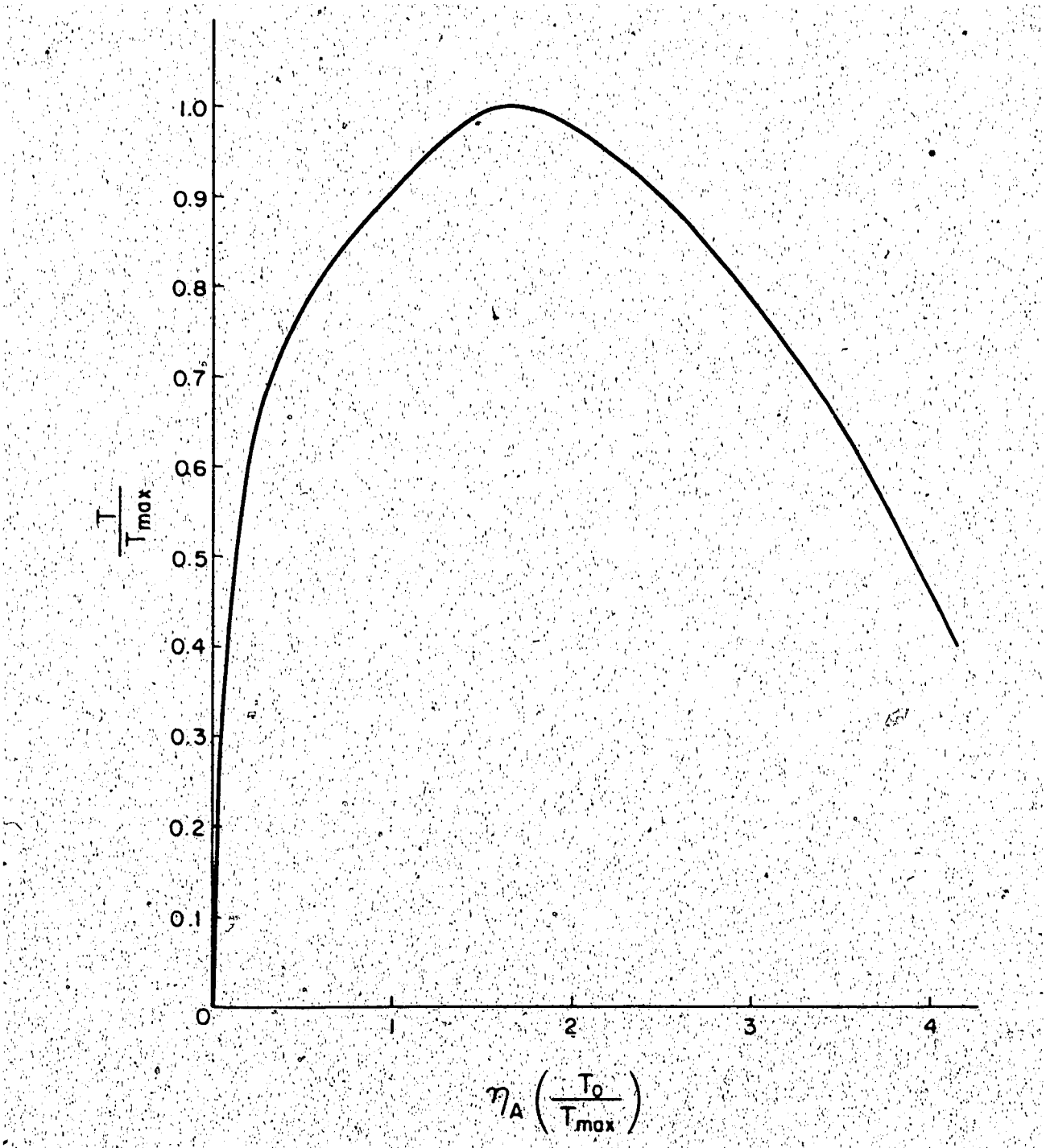

Figure 4.7 Normalized temperature profile vs normalized actual distance.

4.4 Experiment

The convective arc cooling phenomenon was investigated by blowing an arc onto a flat plate with a strong flow of gas. The arc was discharged between a pair of cylindrical steel electrodes which were axially mounted on the opposite sides of a Delrin test section described in Section 3.3. The electrodes were mounted flushed with the delrin walls so that they do not obstruct the flow. An RLC circuit, shown in Figure 3.3, which consisted of three 240 μF, 5 kV capacitors and one 7 mH inductor provided the necessary arc energy. Circuit resistance was adjustable depending on the required current magnitude and rise time. With the chosen electrode gap separation, no self induced electrical breakdown was possible even if the capacitors were charged to the required voltage. A plasma spark plug was installed within the ground electrode to initiate gas breakdown in the electrode gap.

A shock tube and a test section described in Section 3.2 and 3.3 were used to generate the necessary air flow. Ceramic plates constructed in single, double or multiple stack configurations were installed within the test section for various experiments.

The events of arc discharging and gas flow initiation were synchronized by using electronic triggering. The arrival of a shock wave was detected by a pressure

transducer whose signal actuated the external trigger of the Tektronix 556 oscilloscope. A gate pulse from the oscilloscope was delivered to a delay pulse unit which in turn triggered the plasma plug circuit to fire the plasma plug. An illustration is given in Figure 4.8.

The plasma plug was fired at such a time that the arc current would just reach a maximum magnitude when the shock wave arrived at the testing sections. The arc thus appeared to be in a DC state at the moment when it was swept downstream by the gas flow.

The flow pattern of the arc was recorded by both the streak camera and a conventional Polaroid camera. The streak pictures recorded the temporal development of the arc at various locations along the plate surface. The Polaroid picture gave a time integral photograph of the arc. Neutral density filters ranging from 1% to 60% transmission were used to reduce the apparent arc brightness. The voltage gradient of the arc was monitored by two Tektronix P6015 HV probes which were connected to the two electric probes embedded in the ceramic plate. Signals were fed into a differential voltage amplifier installed in the scope. The arc current was measured simultaneously by recording the voltage difference across a 1/6 Ω shunt resistor. Various combinations of arc current and gas flow speed were measured

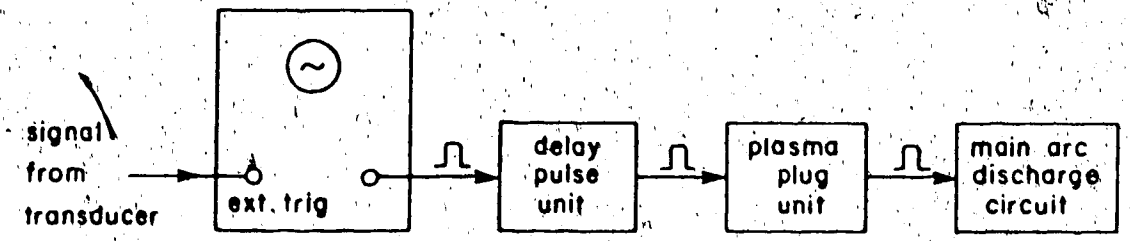

Figure 4.8 Triggering system for the arc discharge.

4.5 Results

The characteristic of an arc convecting over a ceramic plate of length ≈5 cm was first studied. Air was chosen as the flowing medium. A shock speed of Mach ≈1.3 was produced in a shock tube by filling the driver section with air to a pressure of 340 kPa absolute while the driven section was maintained at atmospheric air pressure. The flow speed behind the shock is at 140 m/s.

The arc circuit parameters were chosen to be an inductance of 7 mH, a capacitance of 720 μF and a shunt resistance of 1/6 Ω. The 1.0 cm diameter electrodes were separated at a distance of 3.0 cm. The initial capacitor voltage ranged from 600 V to 2000 V. Both arc voltage gradient and current were monitored.

Typical electrical arc characteristics are shown in Plate 4.1 and Plate 4.2 in the absence and presence of the shock respectively. Without any flow, the arc existed for a duration of 14 ms. The arc voltage attained a magnitude of 160 V, while the arc current reached a maximum amplitude of 340 A. Successive arc current amplitudes decreased with time due to resistive losses. However, as shown in Plate 4.2, the arc current in the presence of flow vanished to zero in a

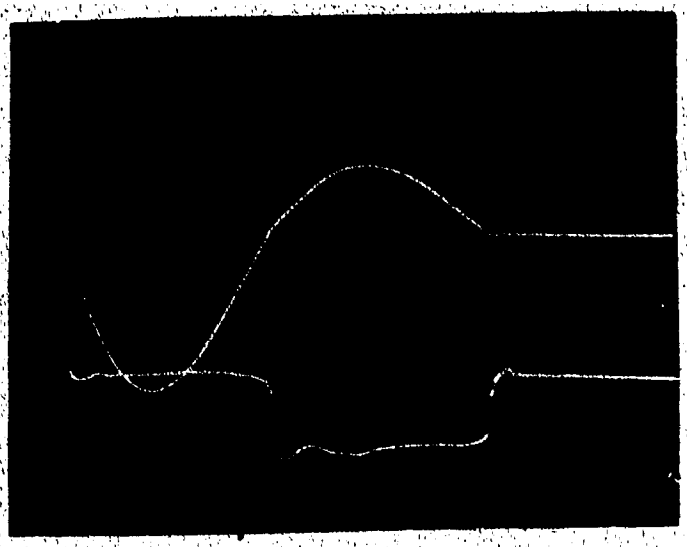

Arc charging voltage : 1 kV

Arc current : 120 A/div

Arc voltage : 200 V/div

2 ms/div

Plate 4.1 Arc current and voltage characteristics without shock.

Arc charging voltage : 1 kv

Arc current : 120 A/div

Differential voltage between probes at 3 cm apart : 50 v/div

0.2 ms/div

Plate 4.2 Arc current and voltage characteristic with shock.

due to the arc current flowing in opposite direction to the order of voltage measurement. A higher electric potential was measured at position two than at position one (as shown in Figure 4.9a). The difference of $V_1 - V_2$ was hence negative. At a later time, the voltage difference reversed sign indicating that the arc had extended and rejoined at the end of the plate. At this time, the electric potential at position one was higher than position two. The voltage difference of V_1 and V_2 became positive (as shown in Figure 4.9b). It was not desirable to have the arc joining at the end of the plate since the arc resistance would be reduced.

The length of the flat plate was extended from 8 cm to 20 cm, while other parameters, namely, voltage, flow speed, circuit parameter values, were kept the same. The positive voltage difference disappeared, as shown in Plate 4.3. The arc current was maintained at 340 A, while the differential arc voltage varied between 100 V and 150 V over a distance of 3 cm. Multiple traces indicated the repeatability of the arc discharge. The line drawn on the plate gives an 'average' variation of the electric field gradient.

The arc current and period of oscillation were changed by varying the series resistance in the discharging circuit

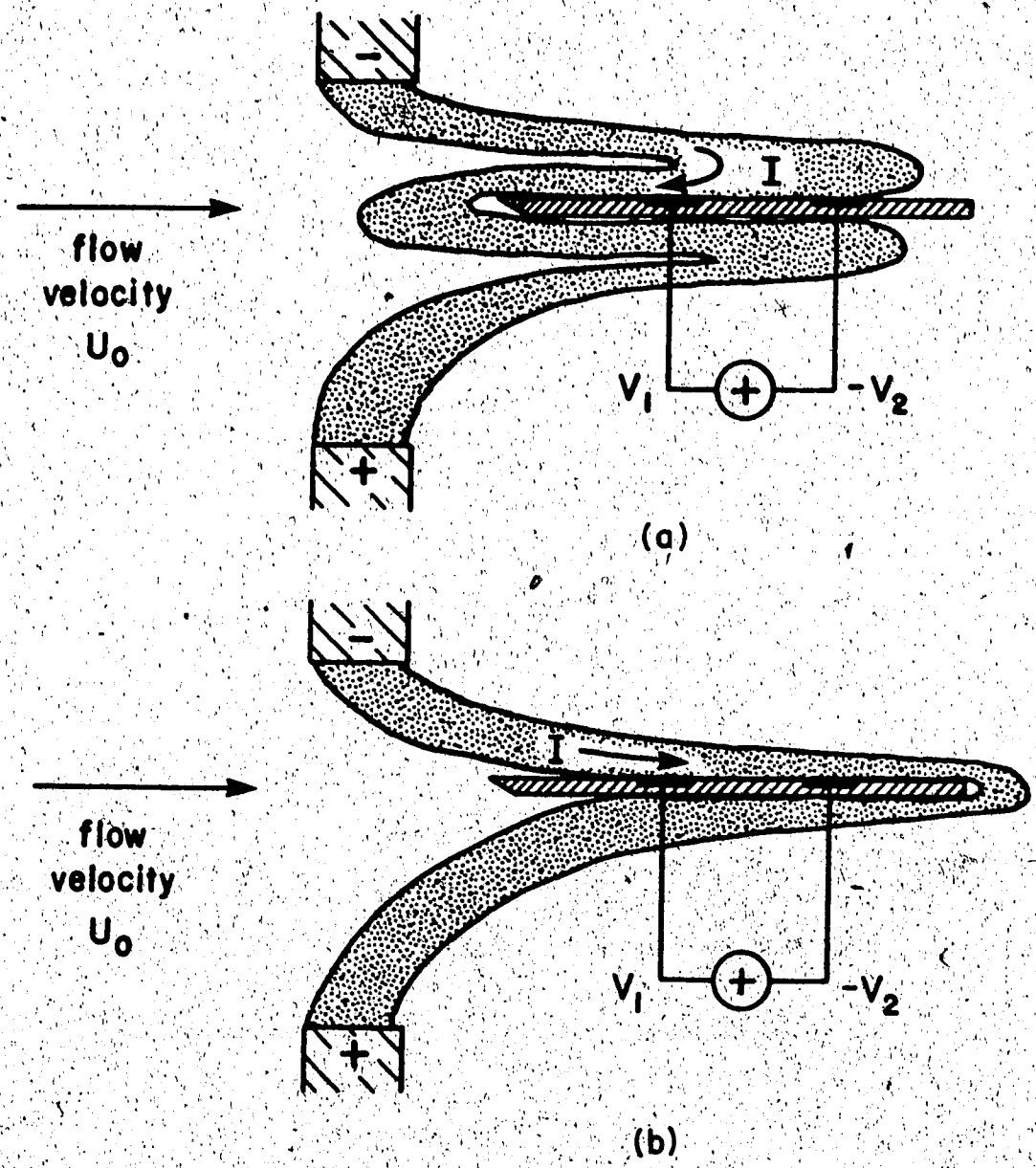

Figure 4.9 Direction of current flow for the electric field measurement.

discharged through an R-L-C circuit can be evaluated by the equation

$$i(t) = -\frac{V}{L\omega}\sin(\omega t)e^{(-Rt)/(2L)} \qquad (4.22)$$

where $\omega = \left[\frac{1}{LC} - \frac{R^2}{4L^2}\right]^{1/2}$. R, L, C are the resistance, inductance and capacitance of the various components. For each series resistor, the arc current and differential voltage were recorded with the initial capacitor voltage varying between 600 V and 2000 V. The electric field was found to be fairly independent arc current.

Time integrated pictures of the arc were taken with a Polaroid camera. A typical picture of the arc is shown in Plate 4.4. The thickness of the arc was measured to be ≃1.5 mm.

4.6 Discussion

The two dimensional Prandtl boundary layer equations were solved with a temperature transformation and the field-current characteristics were derived. The time integrated picture of the arc layer at the leading edge of the wedge shows that the arc was not 'cut' by the wedge. Instead, it developed into a boundary layer of which the thickness, in general, follows the hydrodynamic boundary

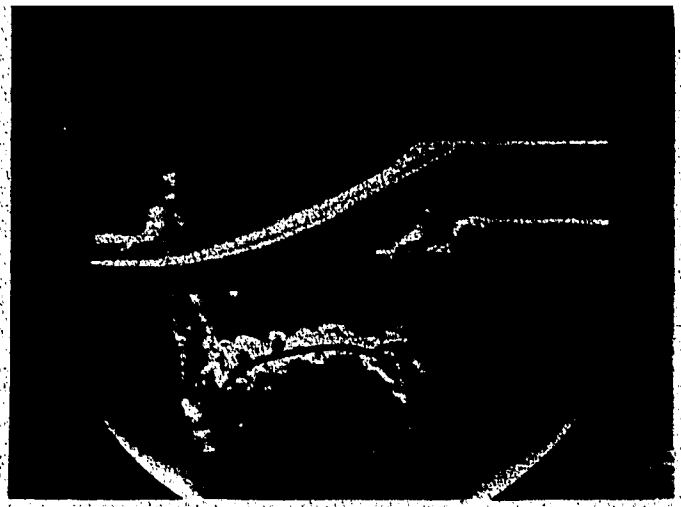

Arc charging voltage : 1 kv

Arc current : 120 A/div

Differential voltage between probes at 3 cm apart : 50 v/div

0.2 ms/div

Plate 4.3 Arc current and arc voltage waveforms with an extended plate.

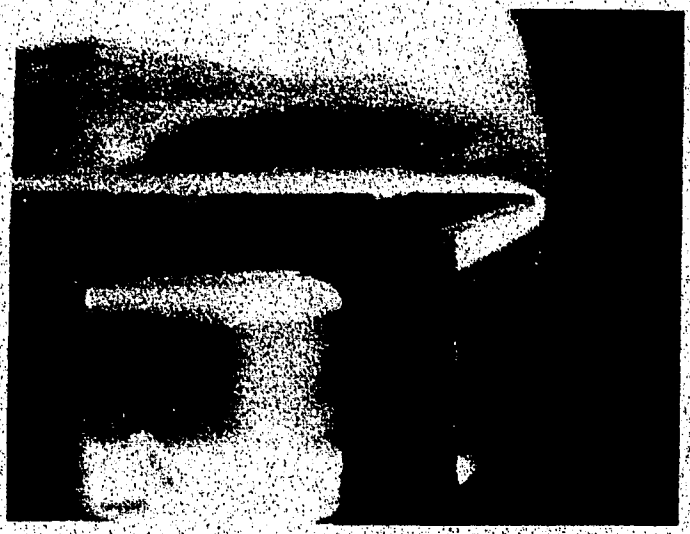

Arc charging voltage : 800 V

Neutral density filter : 2% transmission

Magnification : x 2

Arc thickness : ≃1.5 mm

Plate 4.4 Time integrated picture of an arc.

Measurements of field and current along the plate surface can be found from oscilloscope trace, given in Plate 4.3. The values were normalized with x = 1.5 cm and a flow speed of 140 m/s. The width of the current was estimated according to the aspect ratio given in Table 6-1. Values of σ_0, ν_0, K_0, T_0 were chosen to be those at 300°K and 1 atmospheric pressure.

Normalized values and predicted values are shown in Figure 4.5. Substantial discrepancies are noticed. This can be caused by deviations of the actual flow from laminar flow on the plate surface. Moreover, the model predicts the arc electrical behaviour in a two dimensional situation. However, in the real situation, the flow is three dimensional. A preliminary arc thickness measurement showed that the arc thickness was between 1 and 2 mm thick.

5.1 Outline

The flow of an arc in a double plate and a multiple plate system is considered. Theoretical results of the arc temperature profiles and electric field-current characteristics are presented. Experimental data obtained from streak photographs and frame pictures are compared to the predictions of the theory.

5.2 Introduction

The flow of a layered arc on a flat plate was studied in Chapter Four. For the present discussion, a more realistic situation resembling air circuit breakers with chutes made of stacks of separated plates is considered. The penetration of an arc into various channels of the separated plates can be categorized into three cases : (1) The arc flows close to the inner surfaces of a channel near the leading edge and expands into the stream of flow until both layered arcs meet at some point downstream; (2) The arc flows beyond the length of a channel and joins other parts of the arc from other channels so that it forms a single arc layer filling the same channel; (3) A single transverse arc formed upstream does not enter the gap. These three situations were studied via a double plate and a multiple

current characteristics were measured for individual cases. Records of streak pictures were taken for case 2. Framing pictures for the 3 cases were individually taken. The recorded profiles were compared to the theoretical ones and were found to be in good agreement.

5.3 Theory

5.3.1 Case 1 : Double plate configuration with 'in and out' current loop

Figure 5.1 illustrates the two layered arcs expanding into the stream of flow and meeting at some point downstream. The arc thickness at which the two arcs meet is approximated from Figure 4.7 by the non-dimensionalized distance from the wall. Assuming that the arcs meet at the point where the arc peripheral temperature is near the maximum arc core temperature, the non-dimensionalized distance from the wall is given as

$$\eta_A \left[\frac{T_0}{T_{max}} \right] \simeq 2 \qquad (5.1)$$

where $\eta_A = y \left[\frac{U_0}{\nu_0 x} \right]^{1/2}$.

The maximum arc core temperature can be determined by

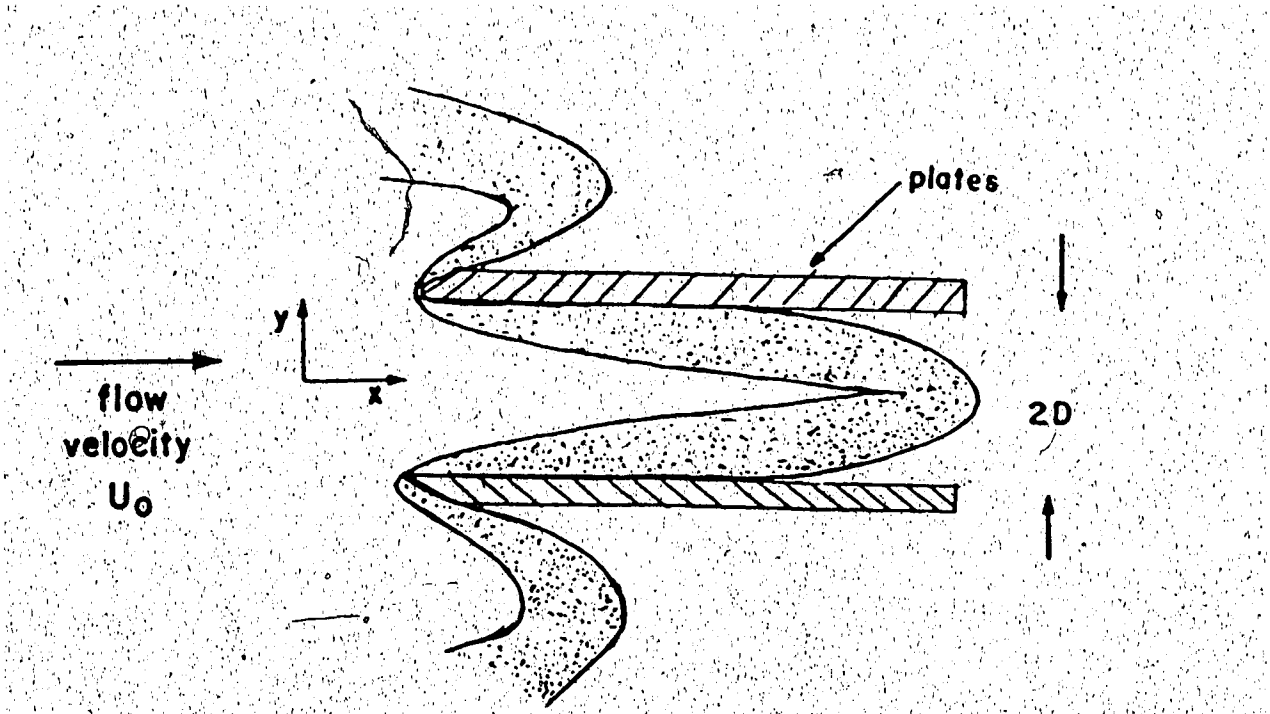

Figure 5.1 Joining of the two boundary layered arcs between a double plate gap.

through η_A. For a known flow speed, the maximum temperature is proportional to the channel width. In other words, a high temperature arc can only enter a gap with a width which allows the appropriate maximum arc temperature.

The transverse electric field between the leading edges of the parallel wedges can be derived from Equation 4.20. By transposing terms in Equation 4.20, the electric field along the plate surface is given as

$$E_x \left[\frac{\sigma_0 \nu_0}{U_0 K_0 T_0}\right]^{1/2} = \frac{I}{J\sqrt{(K_0 \sigma_0 T_0 x)}} \qquad (5.2)$$

where $J = \int_0^\infty \phi^{5/4}\, 60^{-26/\sqrt{\phi}}\, d\eta$

and E_x is the electric field in the same direction along the surface. Although η has a finite limit within the wedge, it is assumed that the limits can be extended to infinity since the integrand becomes very small when η is greater than six according to Figure 4.4. The voltage drop across the half gap width D is equal to the intergral of the electric field E_x over the arc portion starting from the leading edge to where the two boundary layers meet.

$$V_y = \int_0^{x_D} E_x \, dx$$

$$= \frac{2I}{J\sqrt{(K_0 \sigma_0 T_0)}} \left[\frac{U_0 K_0 T_0 x_D}{\sigma_0 \nu_0} \right]^{1/2} \qquad (5.3)$$

where x_D is the location at which the two boundary layers meet. x_D can be found by substituting the half gap width D into Equation 5.1, giving

$$x_D^{1/2} = \frac{D}{2} \left[\frac{U_0}{\nu_0} \right]^{1/2} \left[\frac{T_0}{T_{max}} \Big|_{y=D} \right] \qquad (5.4)$$

Substituting Equation 5.4 into Equation 5.3, the non-dimensionalized field gradient across the gap of width 2D is

$$E_\perp \left[\frac{\nu_0}{U_0} \right] \left[\frac{\sigma_0}{K_0 T_0} \right]^{1/2} = \frac{I}{J\sqrt{(K_0 \sigma_0 T_0 \phi_{max})}} \qquad (5.5)$$

The integral J can be evaluated directly from Figure 4.5. Results of the field current characteristic are shown in Figure 5.2(case 1).

5.3.2 Case 2 : Multiple plate configuration with unidirectional current

Under conditions of high speed flow, the arc entering a multiple plate system does not necessarily close within the

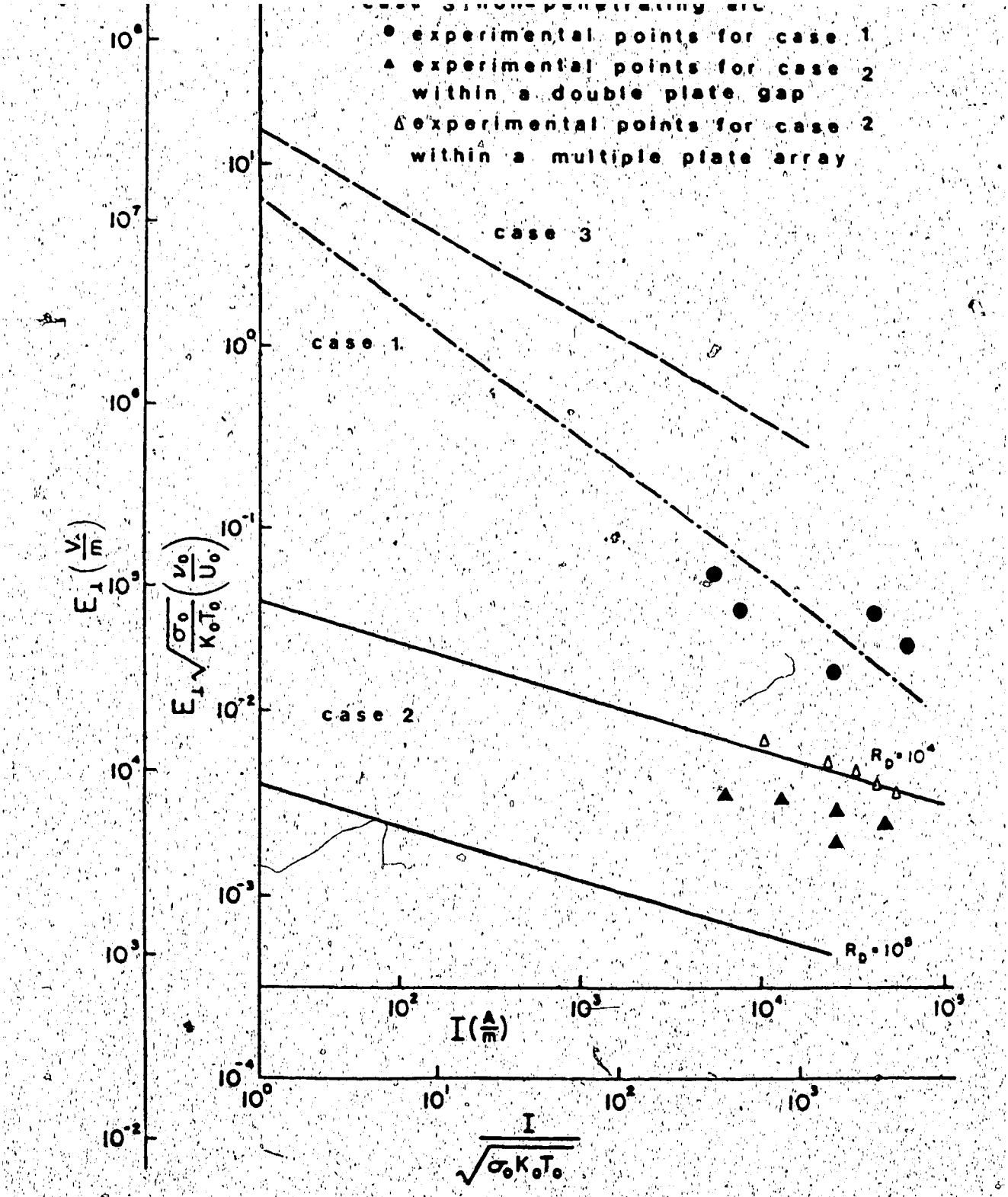

Figure 5.2 Normalized electric field versus current for the 3 cases.

double plate system. Instead, it can stretch beyond the plate and join another part of the arc which flows through a different channel. Such arc configuration is shown in Figure 4.9 and is considered briefly.

Assuming that pressure remains constant, the flow will be axial and constant. The heat flow equation then reduces to a simple balance of heat conduction losses along the y-axis and joule heating, namely,

$$\frac{\partial}{\partial y}\left[K\frac{\partial T}{\partial y}\right] = -\sigma E^2 \qquad (5.6)$$

Using a temperature transformation variable for y,

$$dy = \frac{T}{T_0}dy_0 \qquad (5.7)$$

and conductivity

$$\sigma = \sigma_0\left[\frac{T}{T_0}\right]^{3/2} 60^{-26/(T/T_0)} \qquad (5.8)$$

Equation 5.6 is converted into the form,

$$\frac{d^2\phi}{dy_0^2} = -\frac{2\sigma_0 E^2}{K_0 T_0}\phi^{5/4} 60^{-26/\sqrt{\phi}} \qquad (5.9)$$

where $\phi = \left[\frac{T}{T_0}\right]^2$.

By letting $Y = y_0\left[\frac{2\sigma_0 E^2}{K_0 T_0}\right]^{1/2}$ and scaling ϕ with the maximum

arc core temperature T_{max}, Equation 5.9 becomes

$$\frac{d^2W}{dY^2} = - \left[\frac{26}{x}\right]^{1/2} W^{5/4} 60^{-x/\sqrt{W}} \qquad (5.10)$$

where : $W = \frac{\phi}{\phi_{max}}$, $x = 26\left[\frac{T_0}{T_{max}}\right]$.

Equation 5.10 is solved with the boundary condition that the arc temperature reaches a maximum at the centre of the channel and drops to zero at the wall. Figure 5.3 shows the temperature and electrical conductivity profile within the channel. The current per unit width parallel to the surface is

$$I = 2\int_0^{y_{max}} \sigma E \, dy \qquad (5.11)$$

where y_{max} is half the separation of the channel plates. In terms of the temperature scaled distance dy_0, Equation 5.11 is reduced to

$$I = 2\int_0^{y_{0\,max}} \sigma E \frac{T}{T_0} \, dy_0 \qquad (5.12)$$

Assuming an average temperature $\bar{T}$ across the channel, $y_{0\,max}$ can be found from Equation 5.7 as

$$y_{0\,max} = \frac{T_0 D}{\bar{T}} \qquad (5.13)$$

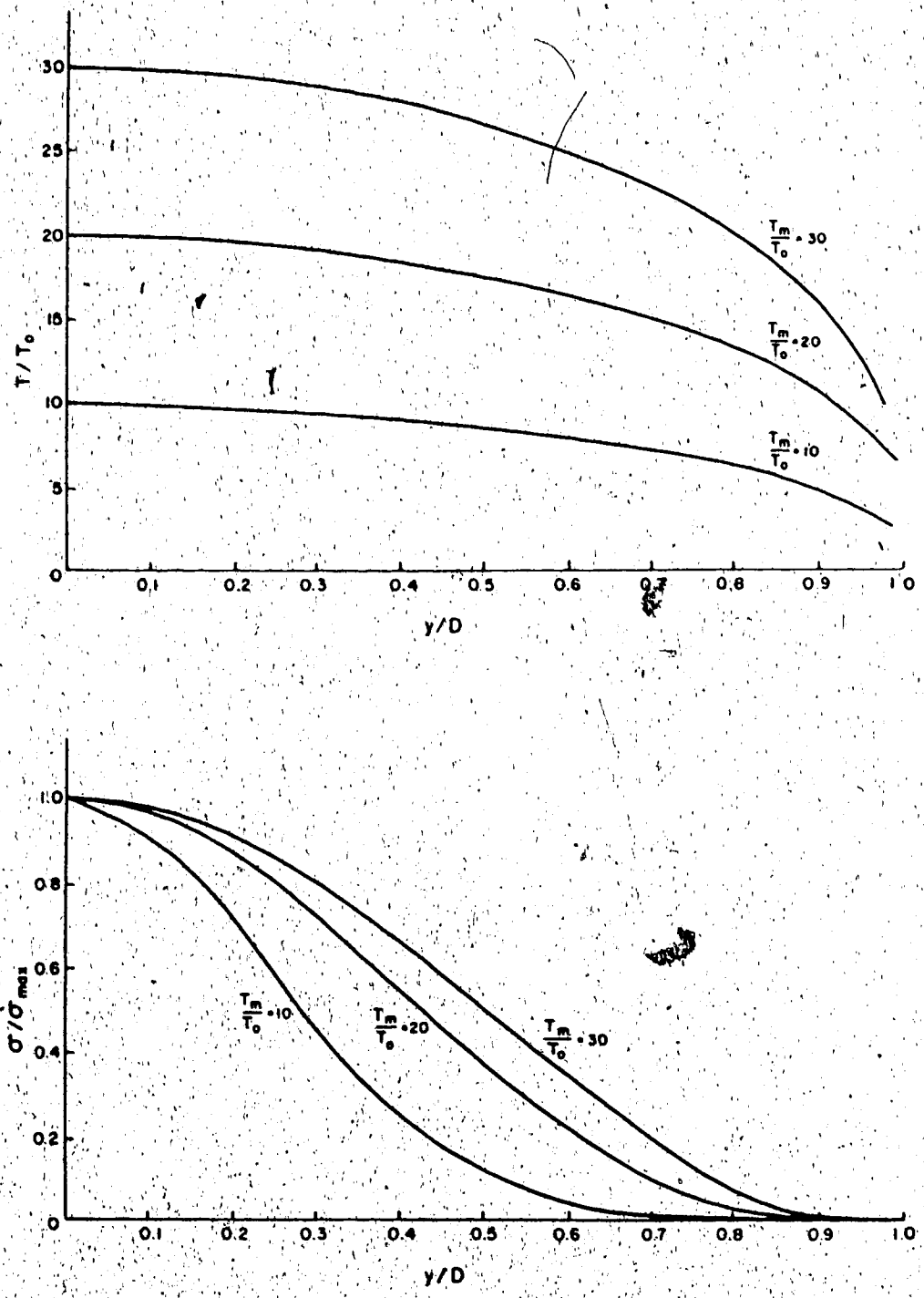

Figure 5.3 Normalized temperature and conductivity within half the gap.

where D is the half gap width of the double plate system. Normalizing Equation 5.12 and using Equation 5.8, the current becomes :

$$I = \frac{2D\sigma_0 E}{\sqrt{\phi}} \int_0^1 \left[\frac{T}{T_0}\right]^{5/2} 60^{-26/(T/T_0)}\, dy' \qquad (5.14)$$

where : $\sqrt{\phi} = \left[\frac{T}{T_0}\right]$ and $dy' = dy_0 / \left[\frac{D}{\sqrt{\phi}}\right]$.

Introducing the normalized quantity, $W = \frac{\phi}{\phi_{max}}$ and $x = 26\frac{T_0}{T_{max}}$ into Equation 5.14, the current becomes :

$$I = \frac{2D\sigma_0 E}{\sqrt{\phi}} \int_0^1 W^{5/4} \left[\frac{26}{x}\right]^{5/2} 60^{-x/\sqrt{W}} dy' \qquad (5.15)$$

With $Y = y_0 \left[\frac{2\sigma_0 E^2}{K_0 T_0}\right]^{1/2}$ and $dy_0 = \left[\frac{D}{\sqrt{\phi}}\right] dy'$,

Equation 5.15 can be further modified to :

$$\frac{I}{\sqrt{K_0 T_0 \sigma_0}} = \sqrt{2}\left[\frac{26}{x}\right]^{5/2} \int_0^{Y_{range}} W^{5/4}\, 60^{-x/\sqrt{W}}\, dY \qquad (5.16)$$

where :

$$Y_{range} = \sqrt{\left[\frac{2\sigma_0 E^2 D^2}{K_0 T_0}\right]} / \sqrt{\phi} \qquad (5.17)$$

The electric field can be evaluated from Equation 5.17 as :

$$E = Y_{range} \sqrt{\phi} \left[\frac{K_0 T_0}{2\sigma_0 D^2} \right]^{1/2} \qquad (5.18)$$

In terms of the normalized quantity, $W = \frac{\phi}{\phi_{max}}$, the electric field can be expressed as :

$$E_{\perp} \left[\frac{\nu_0}{U_0} \right] \left[\frac{\sigma_0}{K_0 T_0} \right]^{1/2} = \frac{Y_{range}}{1.414 R_D} \left[\frac{26}{x} \right] W^{1/2} \qquad (5.19)$$

where R_D is the Reynold's number $\frac{u_0 D}{\nu_0}$.

A family of field-current characteristics for different Reynolds numbers are shown in Figure 5.2(case 2)

5.3.3 Case 3 : Multiple plate configuration in which arc is formed upstream but does not penetrate into the channels

A stack of multiple plates in the main stream flow acts as a physical block against the flow. As a result, the flow speed within the channels increases leading to an enhancement of convective cooling. The plates act as efficient heat sinks to the arc. Due to higher heat losses within the multiple channels, the arc does not enter the stack.

A simple and idealized model is constructed to describe such a case. It is shown in Figure 5.4 where cold gas flows from the left at a velocity U_0, pushing the arc against the stack plates. The properties of the gas and their functional dependence on temperature are assumed to be the same as before. The flow is considered to be one dimensional with mass flow ρu being conserved. Under these conditions, the energy equation which takes the form of :

$$\rho c_p u \frac{\partial T}{\partial x} = \frac{\partial}{\partial x}\left[K \frac{\partial T}{\partial x}\right] + \sigma E^2 \qquad (5.20)$$

is converted into the equation

$$\frac{d^2\phi}{dx_0^2} = \frac{\rho_0 c_{po} u_0}{K_0} \frac{d\phi}{dx_0} - \frac{2\sigma_0 E^2}{K_0 T_0} \phi^{5/4} 60^{-26/\sqrt{\phi}} \qquad (5.21)$$

where : $\phi = \left[\frac{T}{T_0}\right]^2$.

Non-dimensionalizing the equation with the half gap width D, Equation 5.21 reduces to :

$$\frac{d^2\phi}{dx'^2} = R_D P_R \frac{d\phi}{dx'} - A_D \phi^{5/4} 60^{-26/\sqrt{\phi}} \qquad (5.22)$$

where $x' = \frac{x_0}{D}$, $R_D = \frac{U_0 D}{\nu_0}$,

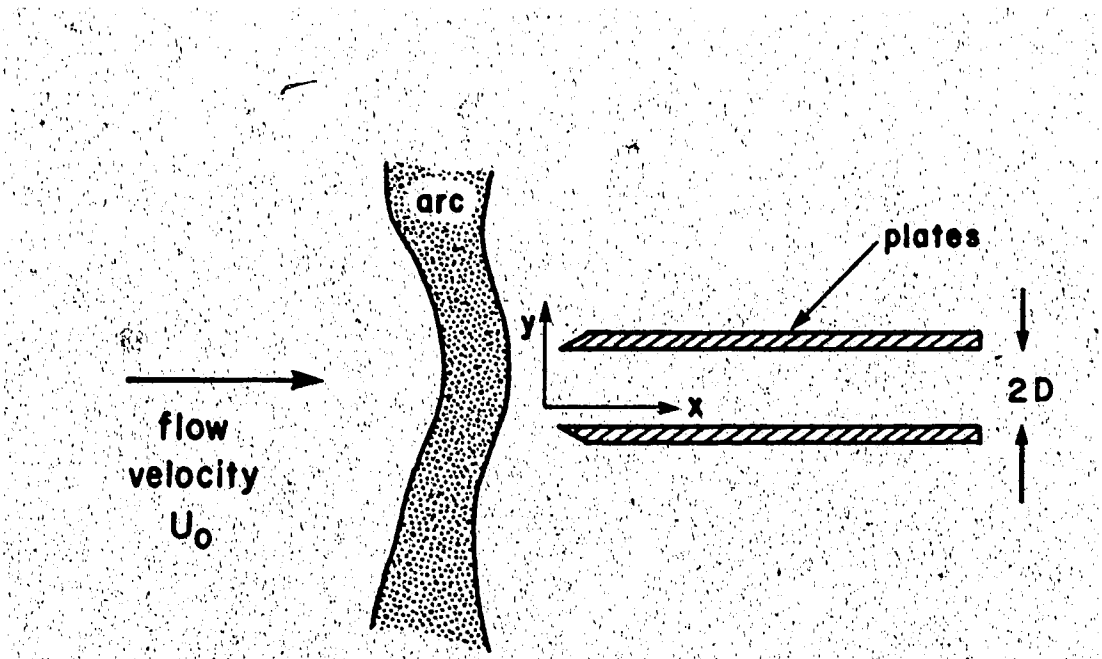

Figure 5.4 Non-penetrating arc in front of the wedge.

$$P_R = \frac{\rho_0 c_{p0} \nu_0}{K_0}, \quad A_D = \frac{2\sigma_0 E^2 D^2}{K_0 T_0}$$

Substituting $X = R_D P_R x'$ into Equation 5.22 and letting $W = \frac{\phi}{\phi_{max}}$, Equation 5.22 becomes :

$$\frac{d^2W}{dX^2} = \frac{dW}{dX} - \frac{A_D \phi_{max}^{1/2}}{(R_D P_D)^2} W^{5/4} 60^{-26/\sqrt{W \phi_{max}}} \qquad (5.23)$$

With the boundary conditions that $x = 0$, $W = 1.0$, $W' = 0.0$, solutions of W at the arc front are found for various combinations of the constant $\frac{A_D}{(R_D P_R)^2} \phi_{max}^{1/2}$. A plot of the normalized temperature is shown in Figure 5.5. The electric field can be determined from the constant A_D as :

$$ED\left[\frac{\sigma_0}{K_0 T_0}\right]^{1/2} = \left[\frac{A_D}{2}\right]^{1/2}. \qquad (5.24)$$

The current per unit arc width is given by the integral across the arc thickness as

$$\frac{I}{\sqrt{\sigma_0 K_0 T_0}} = \frac{\sqrt{A_D/2}}{P_R R_D} \phi_{max}^{5/4} \int W^{5/4} 60^{-26/\sqrt{(\phi_{max} W)}} dX \qquad (5.25)$$

The relation between the electric field and the current is shown in Figure 5.2(case 3).

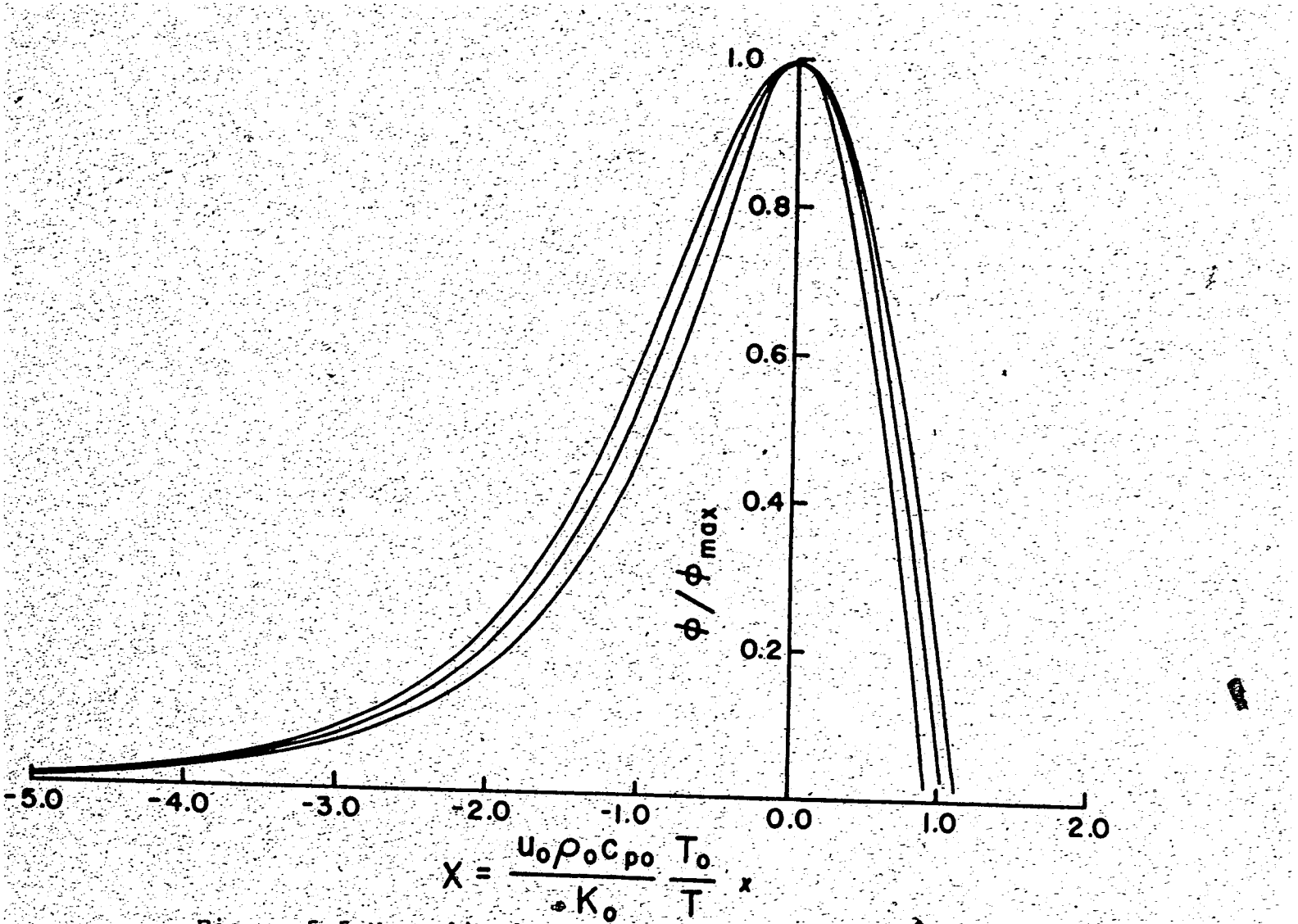

Figure 5.5 Normalized temperature profile of the arc in front of the wedge gap.

5.4 Experiment

5.4.1 Control Parameters

Testing Wedge

A double plate system which was installed along the direction of gas flow replaced the single plate system described earlier. The plates are 20 cm in length. On the bottom plate, as shown in Plate 5.1, two 0.3 cm wide brass strips were embedded at 1.3 cm and 2.3 cm respectively from the leading edge of the plate. At 4.2 cm away from the leading edge, a 1 cm wide brass strip was also set flush into the plate as a ground terminal. The top plate was made from ceramic stove top and later from glass. The glass plate allowed a top view of the arc which flowed between the plates, however, it could not withstand serious thermal stresses from the arc and mechanical stresses from the shock wave. Plate separations varied between 8 mm , 6 mm, 4 mm and 1 mm.

Flow speed control

The gas flow speed within the shock tube was adjusted by varying the initial pressures in the driver and driven sections. Pressure in the driver section was set at either 340 kPa absolute (≃3 atmospheres) for the 25 μm Mylar diaphragm or 600 kPa absolute (≃6 atmospheres) for the 50 μm

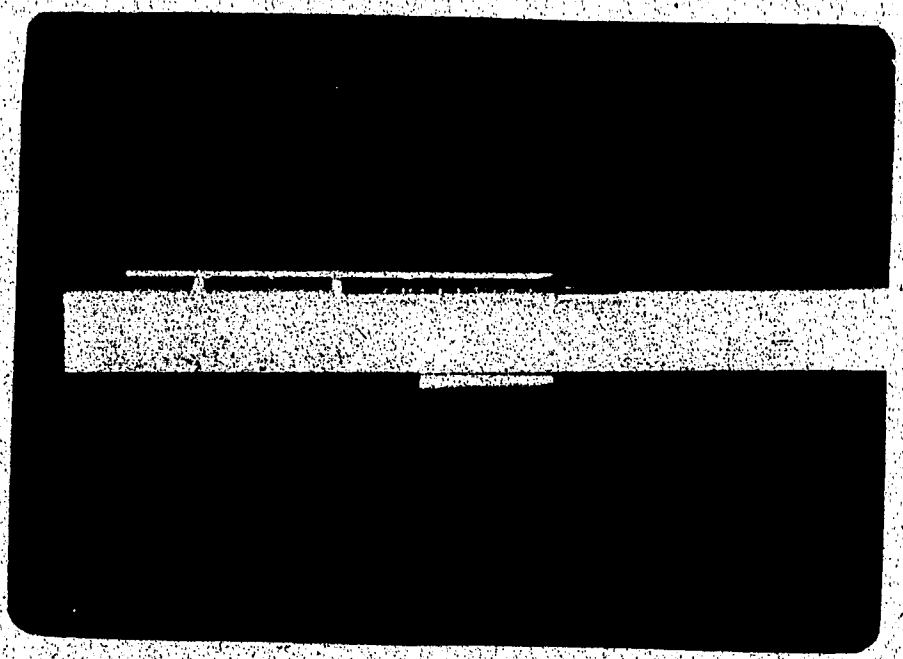

Plate 5.1 Bottom plate of the Delrin test section showing the locations of various electric probes and ground electrode.

Mylar diaphragm. In the driven section, pressure was set at 100 kPa (atmospheric) or 10 kPa (1/10 of atmospheric). A subsonic flow speed of 140 m/s or a supersonic flow speed of 480 m/s could be generated with these pressure combinations.

Arc discharging system

The arc was generated by the discharge of the 720 μF capacitor charged to an initial voltage of between 1000 V to 2000 V (refer to Figure 3.3). Arc current was limited by the series resistance ranging from 100 Ω to 1/6 Ω and an inductance of ≈7 mH. The circuit was discharged at such a time that the current magnitude increased to its peak value upon the arrival of the shock wave. The electrode mounted adjacent to the bottom plate was connected to the high voltage end of the discharging circuit. Such connection guaranteed that the arc would flow close to the plate surface as it was discharged through the downstream ground terminal.

Types of measurements

Two P6015 Tektronix HV probes and a Tektronix 556 dual trace oscilloscope were used to measure the arc voltage, arc current and arc voltage gradient. The arc current was monitored by the voltage drop across a shunt resistor of 1/6 Ω. The voltage gradient was measured by the difference

of voltages monitored from the two brass probes on the plate.

The arc width[4] and thickness[5] was optically measured with the streak camera and the SP 2000 camera system. The layout of the optical system is shown in Figure 5.6. Total reflecting mirrors were used to direct the images into the camera. Light intensities were reduced by using neutral density filters. The streak camera recorded the temporal development of a particular arc portion between the two electric probes embedded in the ceramic plate surface. A streaking time of 50 μs was the longest exposure time provided by the camera. Delayed gate pulses from the oscilloscope triggered the camera at preset times after the firing of the shock. With appropriate delay, a 50 μs streak of the arc could be taken at any time during the arc discharge. Streak images were recorded on Polaroid films of ASA 3000 and Kodak sheet negatives 4164 (ASA 320), 4166 (ASA 1250) and 4141 (ASA 400).

A transmission density scale was used to calibrate the intensity distribution of the arc on the film. A streak of the density scale was taken on the same negatives on which arc streaks were recorded. A Vivitar-285 flash mounted in an

---

[4]The arc width is measured in the direction perpendicular to the plate surface and the flow direction.
[5]The arc thickness is measured in a direction parallel to the plate surface and perpendicular to the flow direction.

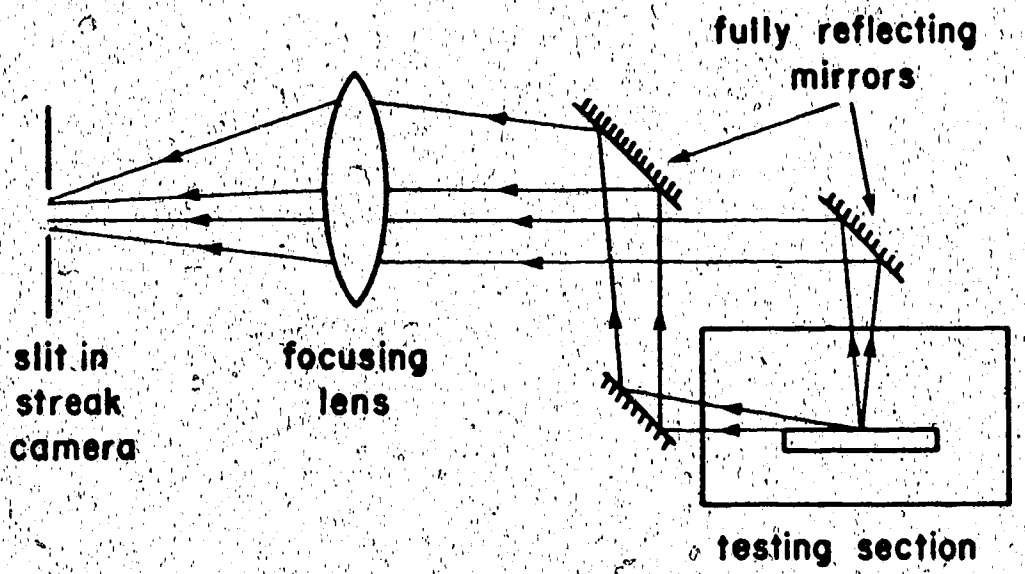

Figure 5.6 Optical arrangements for viewing the arc.

light source for the scale.

Temporal pictures of the complete arc discharge event were taken with the SP 2000 camera at a rate of 2000 frames per second. Each picture recorded the arc for a duration of 0.5 ms. All pictures were stored on magnetic tapes and could be played back on a video monitor whenever necessary.

5.4.2 Electrical measurements with different circuit parameters and flow speeds

The width of the double plate slot as well as the electrode gap were set initially to 8 mm. Series circuit resistance was kept at 100 Ω. Air flow speed was maintained at 140 m/s in the shock tube by keeping a pressure of 340 kPa absolute in the driver section and atmospheric pressure in the driven section. Plate 5.2 shows the electrical waveform of an arc at a peak current of 12 A and initial charging voltage of 1200 V. The shock arrived at the arc when the arc current reached its peak value. The oncoming gas flow stretched and pushed the arc into the slot. The arc resistance increased due to heat losses through conduction and convection, leading to a decrease in arc current. This event lasted for about 0.3 ms as shown in the plate. At this time the arc front had reached the

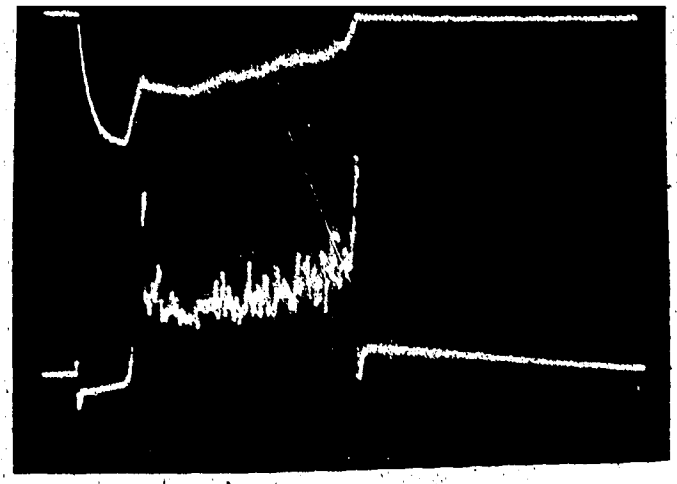

voltage : 1.2 kv

Arc current : 6 A/div

Differential voltage between probes at 1 cm apart : 50 v/div

1 ms/div

(a)

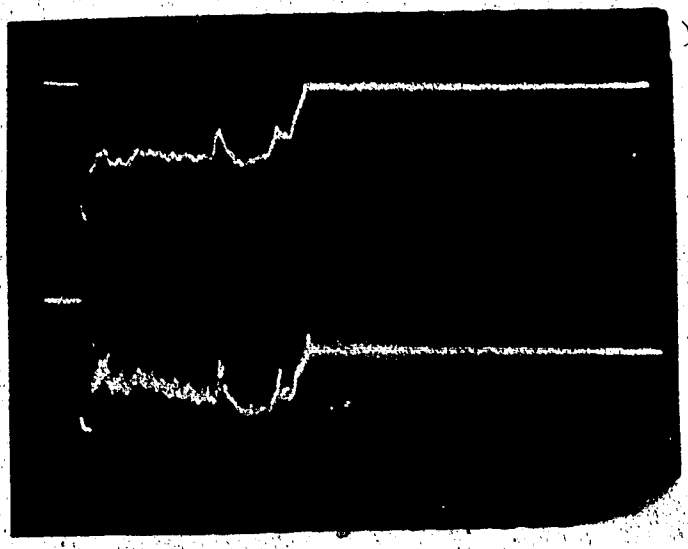

Arc current : 6 A/div

Arc voltage : 500 V/div

5 ms/div

(b)

Plate 5.2 Voltage and current characteristics of an arc with an 8 mm wedge gap.

magnitude on the waveform denoted such a change. After this change, the arc decayed steadily with time as shown by the rest of the oscilloscope trace in the picture. The amplitude of the axial electric field increased steadily from a minimum of 50 V/cm to about 190 V/cm as the current approached zero. Plate 5.2(b) reveals that the arc voltage between the electrodes fluctuated between a magnitude of 200 V and 700 V.

The wedge slot width was reduced to 4 mm with the expectation that the arc would be further confined. Plate 5.3(a) shows a typical arc discharge at 2000 V. The electric field maintained at 50 V/cm throughout the event. Plate 5.3(b) shows an integrated picture of the arc. It can be seen that the arc filled about 2/3 of the gap.

Gas flow speed was increased from 146 m/s to 210 m/s. A peak current of 24 A was generated by discharging an initial arc voltage of 2000 V though a 100 Ω series resistor. The electrodes were set at 8 mm apart. Plate 5.4 shows a typical electrical characteristic of the arc under higher speed flow. Flow speed was further increased to 480 m/s by changing the driving pressure to 600 kPa and the driven pressure to 8 kPa. The electric field measurement was found

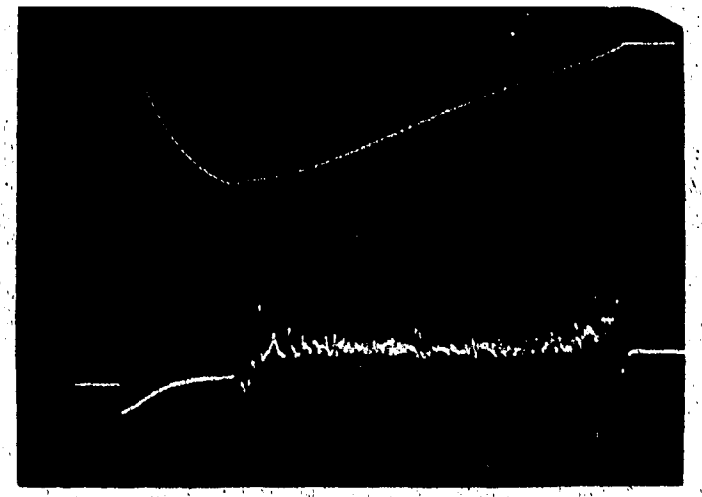

Arc current : 120 A/div

Differential voltage between probes at 1 cm apart : 50 v/div

1 ms/div

(a)

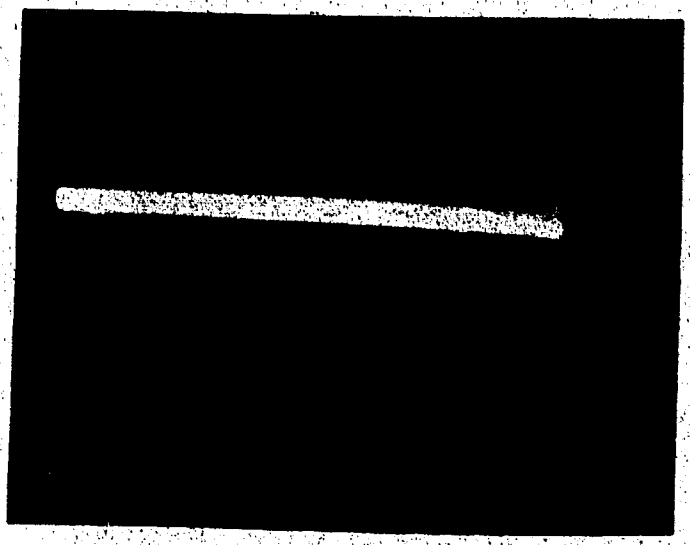

f-stop : f/32

neutral density filters : 1% and 20%

(b)

Plate 5.3 Time integrated picture of an arc between a 4 mm gap.

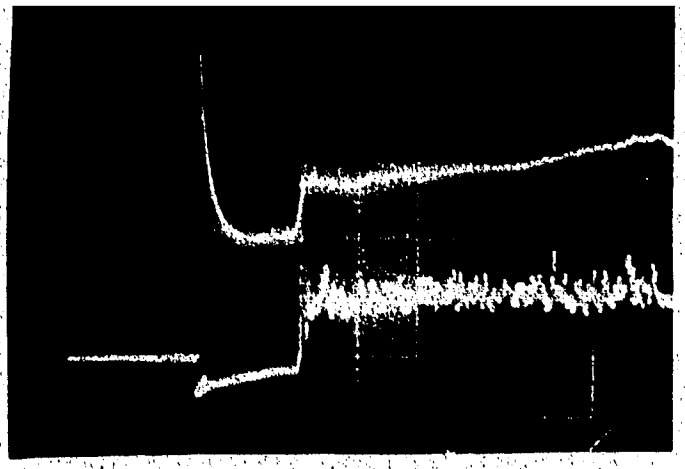

1 ms/div

Arc charging voltage : 2 kv

Arc current : 6 A/div

Differential voltage between probes at 1 cm apart : 50 v/div

Shunt resistor : 100 Ω

Flow speed : 210 m/sec

Plate 5.4 Current and voltage characteristics of an arc between a wedge of 4 mm apart

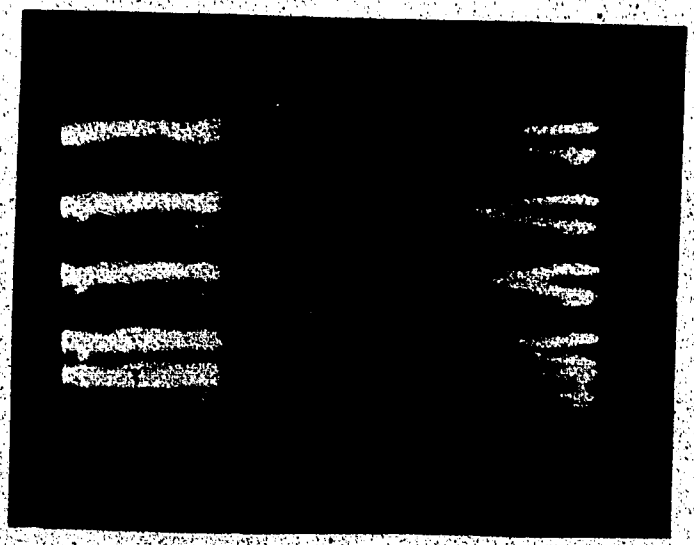

1st trial

2nd trial

Gas Flow

Arc charging voltage : 2 kv

Shunt resistor : 4.3 Ω

Flow speed : 146 m/sec

Exposure duration : 500 ns

Frame interval : 10 μs

f-stop : f/22 (front iris) f/1.2 (back iris)

Taken at 4.2 ms after shock was initiated.

Plate 5.5 Framing pictures of the arc near the leading edge.

(refer to Plate 5.7 shown here).

5.4.3 Records of streak and framing pictures

A better understanding of the geometrical structure of the arc was supplied by the framing and streak pictures. The TRW model 1-D streak camera possessed a framing facility which enabled more detailed information about the arc flow to be obtained. Framing pictures of the arc near the leading edge are shown in Plate 5.5. Two sets of framing pictures were taken 4.2 ms after the shock was initiated. Flow speed was maintained at 140 m/s. The arc was formed with a circuit resistance of 4.3 Ω and initial charging voltage of 2000 V. The electrode gap width was maintained at 8 mm, while the parallel plate gap was fixed at 4 mm. Each frame was exposed for 500 ns with a 10 μs time interval between consecutive frames. The pictures show that the arc stretched into the wedge slot and eventually shorted to the ground terminal forming a single layered arc on the bottom plate surface. Current magnitude was reduced to 20 A by changing circuit resistance from 4.3 Ω to 100 Ω. Unstable layered arcs were formed on the plate as shown in Plate 5,6.

Gas flow speed was raised to 480 m/s* by maintaining a driver section pressure of 600 kPa and a driven section

*See appendix 1

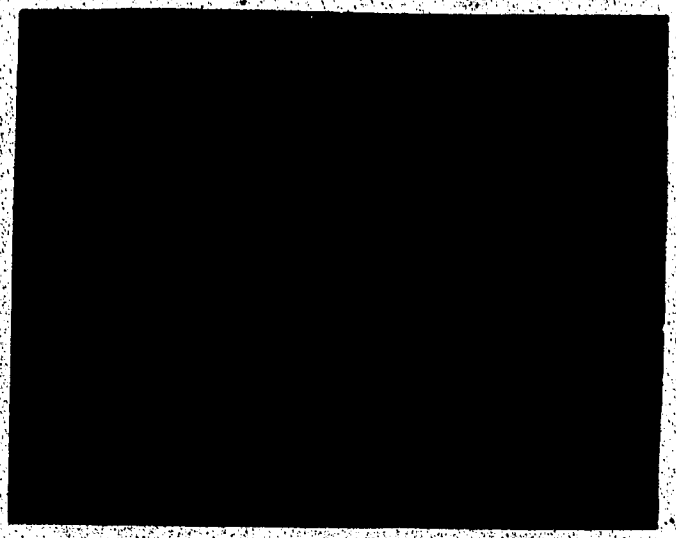

2nd trial 1st trial

Gas Flow

Arc charging voltage : 2 kv

Shunt resistor : 100 Ω

Flow speed : 146 m/sec

Exposure duration : 500 ns

Frame interval : 10 μs

f-stop : f/22 (front iris)
f/1.5 (back iris)

Taken at 4.2 ms after shock was initiated.

Plate 5.6 Framing pictures of an arc at reduced current.

an arc with current magnitude of approximately 200 A and its corresponding electrical characteristic. Streaks of the arc observed from directions perpendicular and parallel to the plate were obtained simultaneously. The uniform streaks indicate that the arc maintained a stable geometrical shape within this period. The voltage gradient parallel to the direction of flow was measured to be about 50 V/cm. The arc width to thickness ratio was measured directly from the picture to be about 3 : 1. It was observed that the physical measurements remained unchanged for other current magnitudes ranging between ≃1680 A and ≃10 A (obtained by reducing series resistance to 1/6 Ω and inductance to 0.51 mH).

5.4.4 Densitometer measurements

The arc width and thickness could be measured more accurately by using the technique of densitometry. For the purpose of scanning the arc intensity distribution, Kodak negatives with film speed ASA 320, 400 and 1250 were used for recording arc streaks. Streaks of the arc thickness, arc width and the transmission density scale were recorded on the same negative. The quality of the streak images was controlled by the choice of the camera slit width, the film types, the neutral density filters for reducing arc

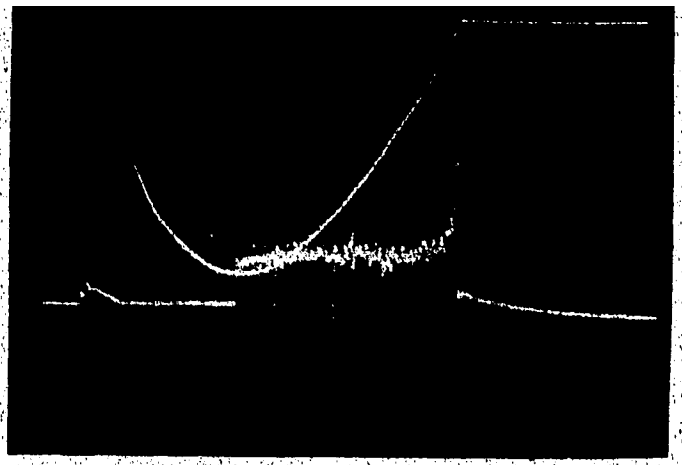

Arc current : 60 A/div

Differential voltage between probes at 1 cm apart : 50 v/div

1 ms/div

Flow speed : 480 m/s

Electrode gap separation : 6 mm

Wedge gap separation : 4 mm

1 ms/div

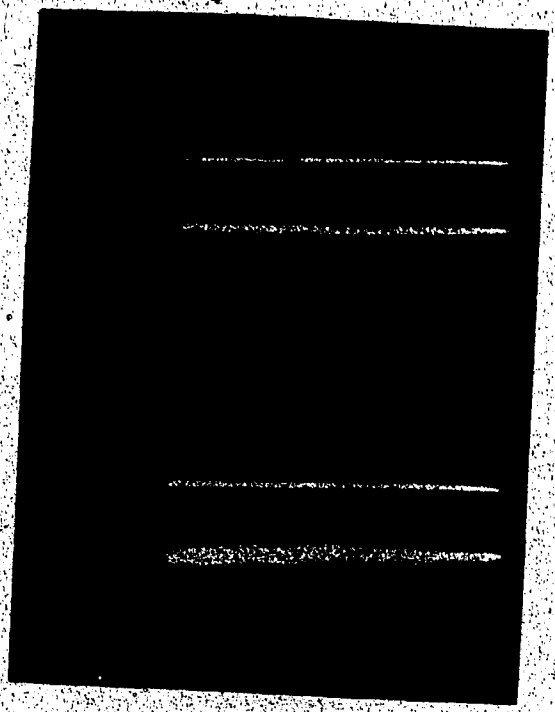

Side view of arc

Top view of arc

Magnification : x 0.2

Taken at 5 ms after shock

50 µs

Plate 5.7 Streak pictures of arcs between a 4 mm wedge gap at a flow speed of 480 m/s.

A discharge of 1 kV through a resistor of $\frac{1}{6}$ Ω created the required arc. Air flow speed was set at 480 m/s. The wedge slot separation and the electrode gap were set at 4 mm and 6 mm respectively. Streak pictures of the arc were taken between the time interval of 3.5 ms and 6.0 ms after the diaphragm in the shock tube burst. It was found that the best streaks of the arc could be obtained by exposing the ASA 1250 sheet film (Kodak Royal X-Pan 4166) with the camera slit set at 0.80 mm. No neutral density filter was required to further reduce the light intensity. The transmission density scale was taken with a slit width of 0.95 mm and at a time of 0.3 ms after the flash was fired at full power. The negatives were developed with Kodak HC-110 developer (dilution A) at a temperature of 20°C for 6 minutes. The developing process was arrested by immersion in a stop bath for 2 minutes and the film was fixed in a fixing bath for 3 minutes.

Plate 5.8 shows a sheet negative of the arc taken at 4.5 ms and 5.0 ms after the shock was initiated. Views parallel and perpendicular to the plate were taken. The transmission density scale was photographed at the moment when the flash light intensity reached a maximum. The negatives were scanned across at distances of 0.2 cm and

Arc charging voltage : 1 kV

Shunt resistor : 1/6 Ω

Side view

Top view

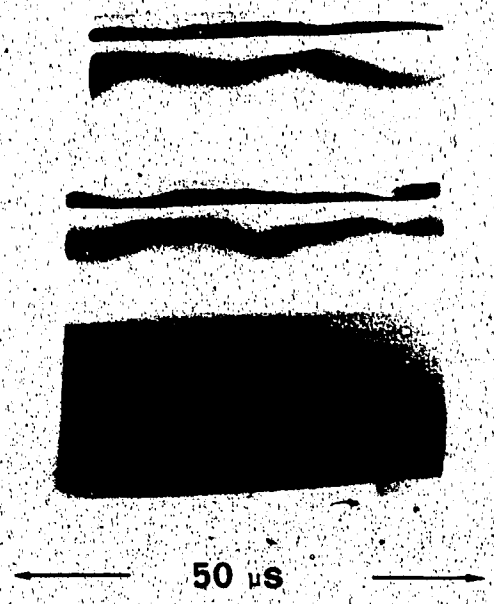

Taken at 4.5 ms after shock was initiated

Taken at 5.0 ms after shock was initiated

Transmission density scale

Plate 5.8 Negative for streaks of an arc between a 4 mm double plate slot.

0.5 cm from the left edge of the streak traces so that good intensity profiles could be obtained. The scanned amplitudes were plotted with a microdensitometer. Scanned profiles of the streaks are shown in Figure 5.7. The scale represents stepwise increases in density' of the film. Each step represents a logarithmic density increment of 0.3 (or $\log_{10}2$) which indicates an increase of incident light power by a factor of two. In terms of f-numbers, each increment corresponds to one f-stop decrease. The arc intensity profiles are calibrated according to this scale. Taking a scanning magnification factor of 5 from the densitometer, and a factor of 1.25 for the object to image magnification, the actual dimensions of the arc became a quarter of the measured values from Figure 5.7.

Since the intensity of the streaks is a result of the total emission from all slices of the arc cross-section, as shown in Figure 5.8, the total intensity from strips near the arc core will be relatively higher than those near the periphery because of the assumed elliptical arc cross-section. The main concern is the light emitted from the side of the arc as it can reveal the thickness of the arc. The intensity of the arc viewed from the side was averaged over the length of the arc strip which is in

---

' Density is defined as the logarithm to base 10 of the ratio of incident light divided by transmitted light

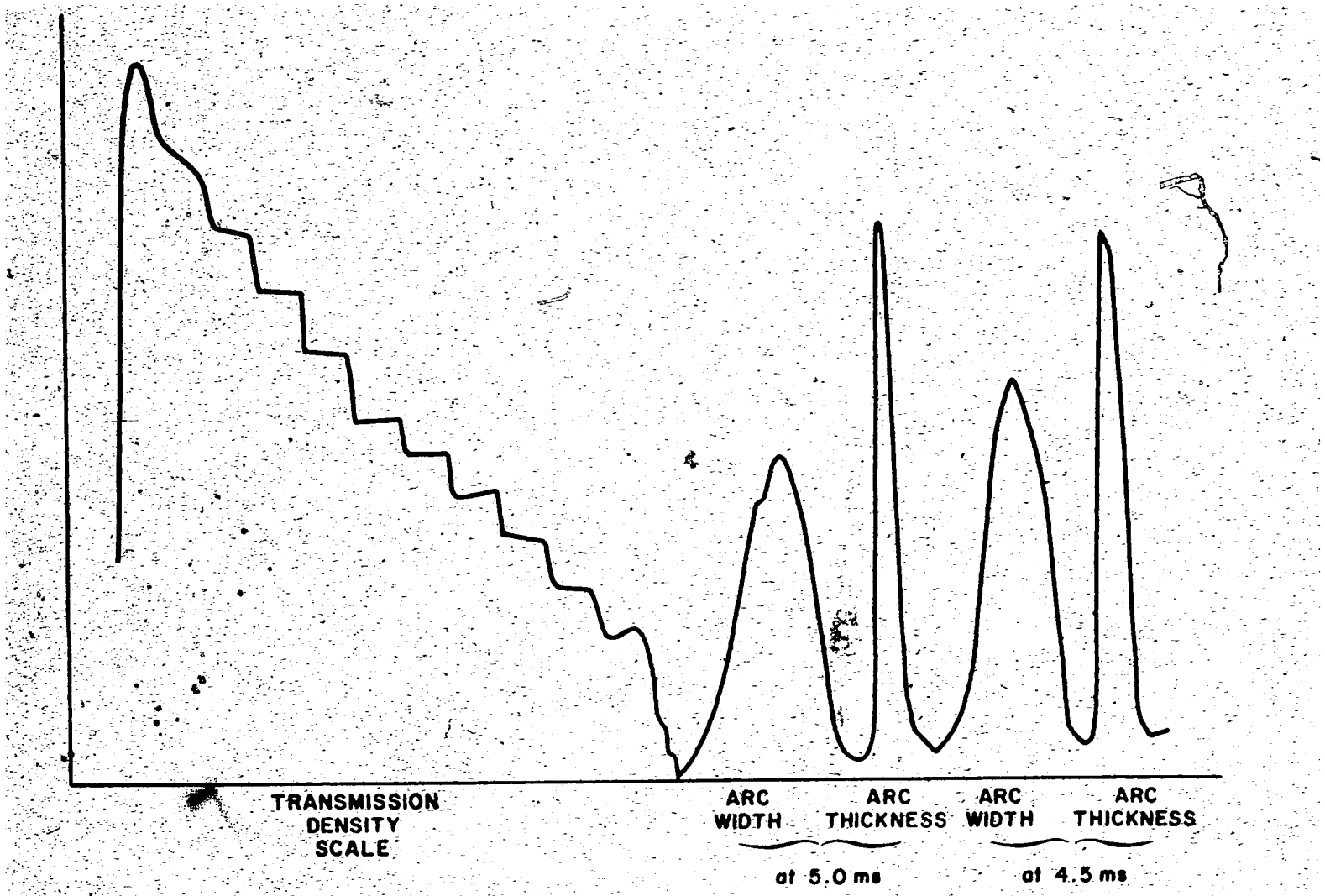

Figure 5.7 Scanned profiles of arc thickness and arc width.

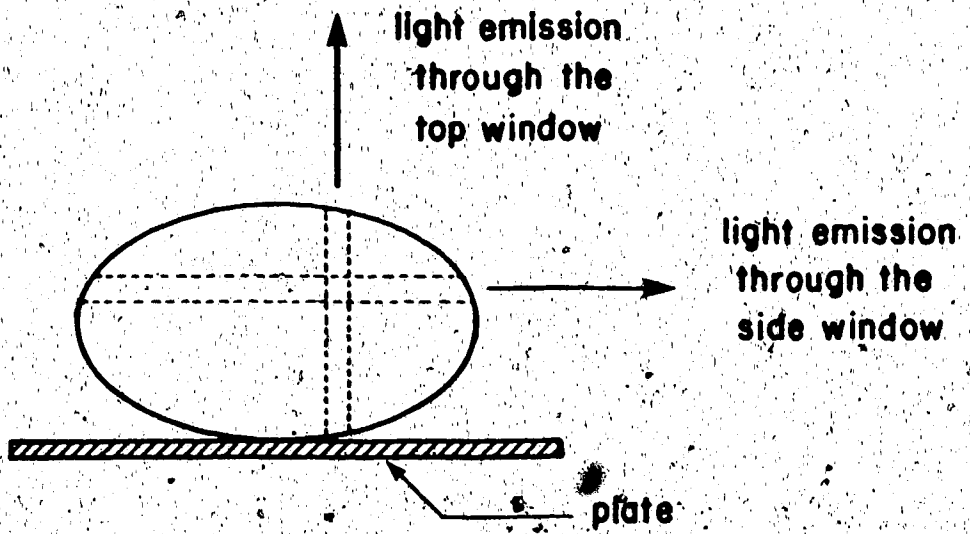

Figure 5.8 Light emission from different sides of the arc.

parallel with the viewing direction. It was further normalized with respect to the maximum value. The normalized intensity versus distance is shown as dots on Figures 5.9 to 5.12. A comparison between the intensity profile and the temperature profile is discussed in Section 5.4.7.

5.4.5 Framing pictures from Spin Physics 2000 high speed camera

Framing pictures of the arc were also taken with the Spin Physics 2000 high speed camera at intervals of 0.5 ms and are shown in Plate 5.9. Flow speed and arc control parameters were the same as those mentioned in section 5.4.4. The width of the arc near the leading edge was observed to spread out downstream in the direction transverse to the gas flow and parallel to the plate.

5.4.6 Multiple plates measurement

A multiple stack of six 5 cm x 6 cm x 0.3 cm glass plates with an interspatial separation of 2 mm, as shown in Plate 5.10, was installed in the test section. Two 3 mm wide brass strips were embedded at a distance of 1.4 cm and 2.4 cm from the leading edge of the plate. Arc electrodes located in front of the leading edge were either separated at a distance of 6 mm or at 2.2 cm which was the same level as the top and bottom plates. Experimental parameters were

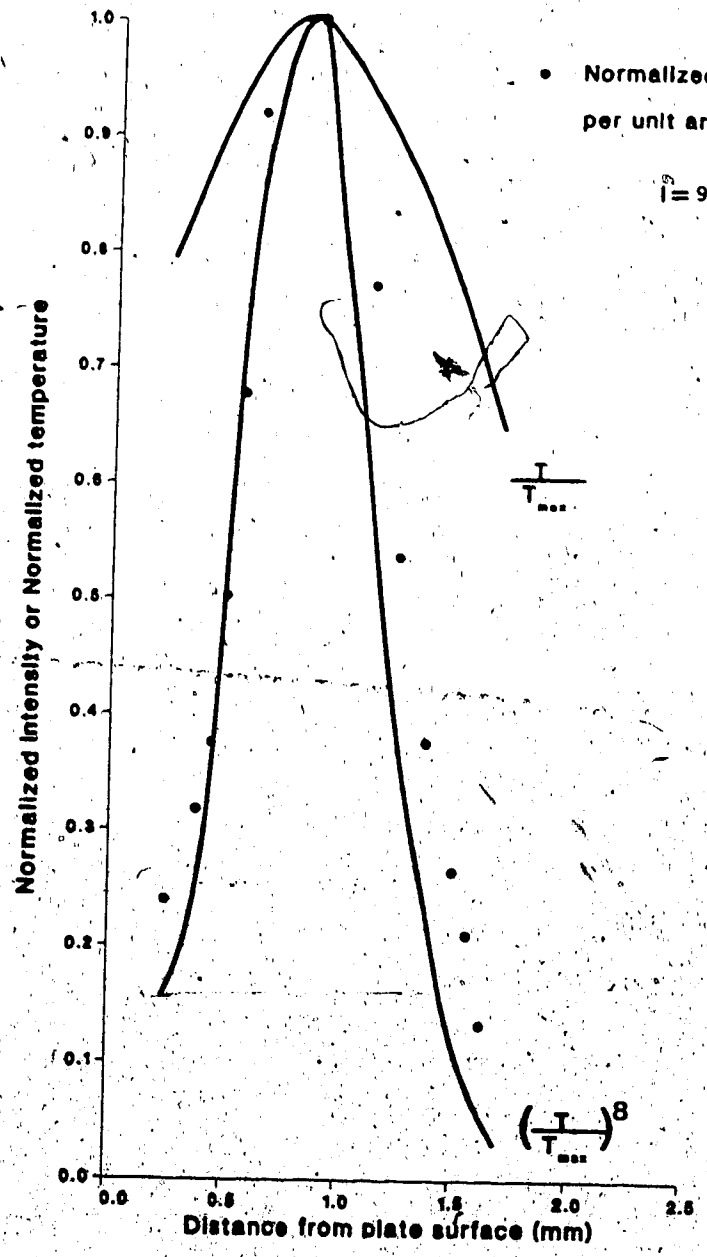

Figure 5.9 Spatial variation of normalized intensity per unit arc width for a current of 96 A.

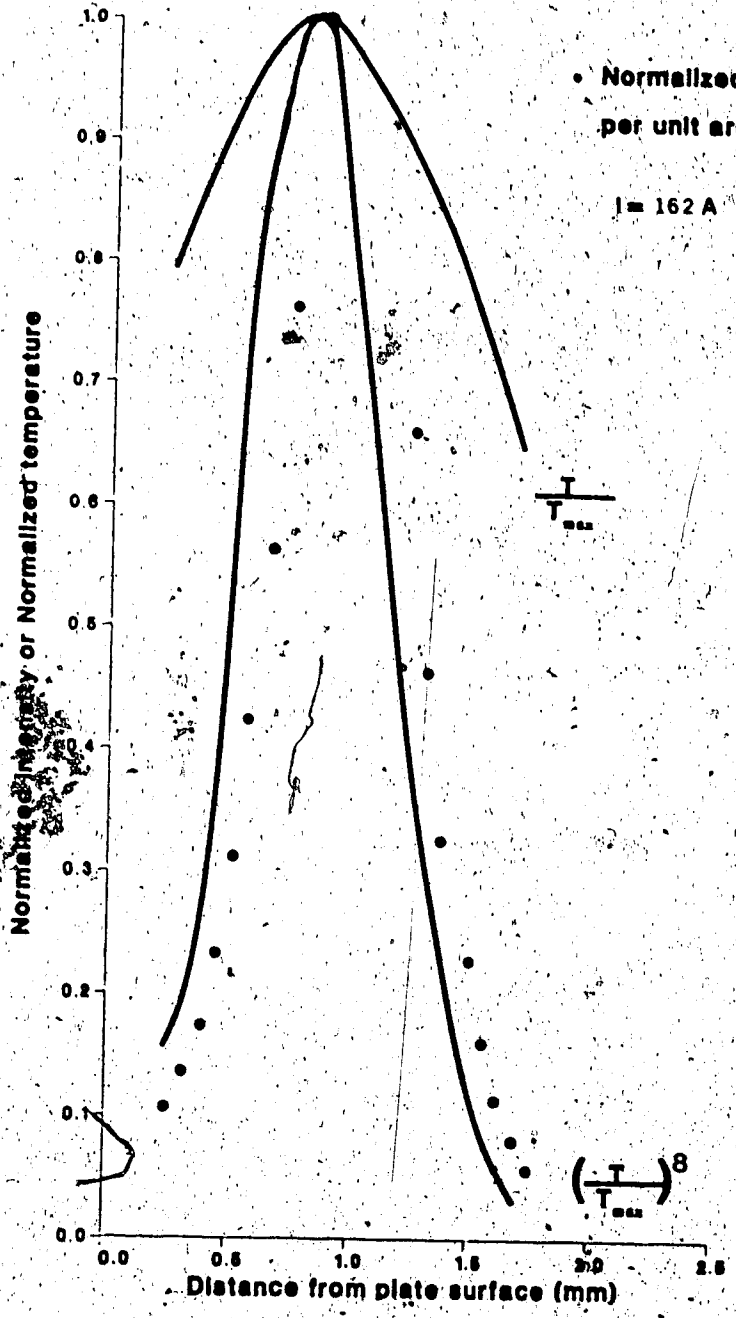

Figure 5.10 Spatial variation of normalized intensity per unit arc width for a current of 162 A.

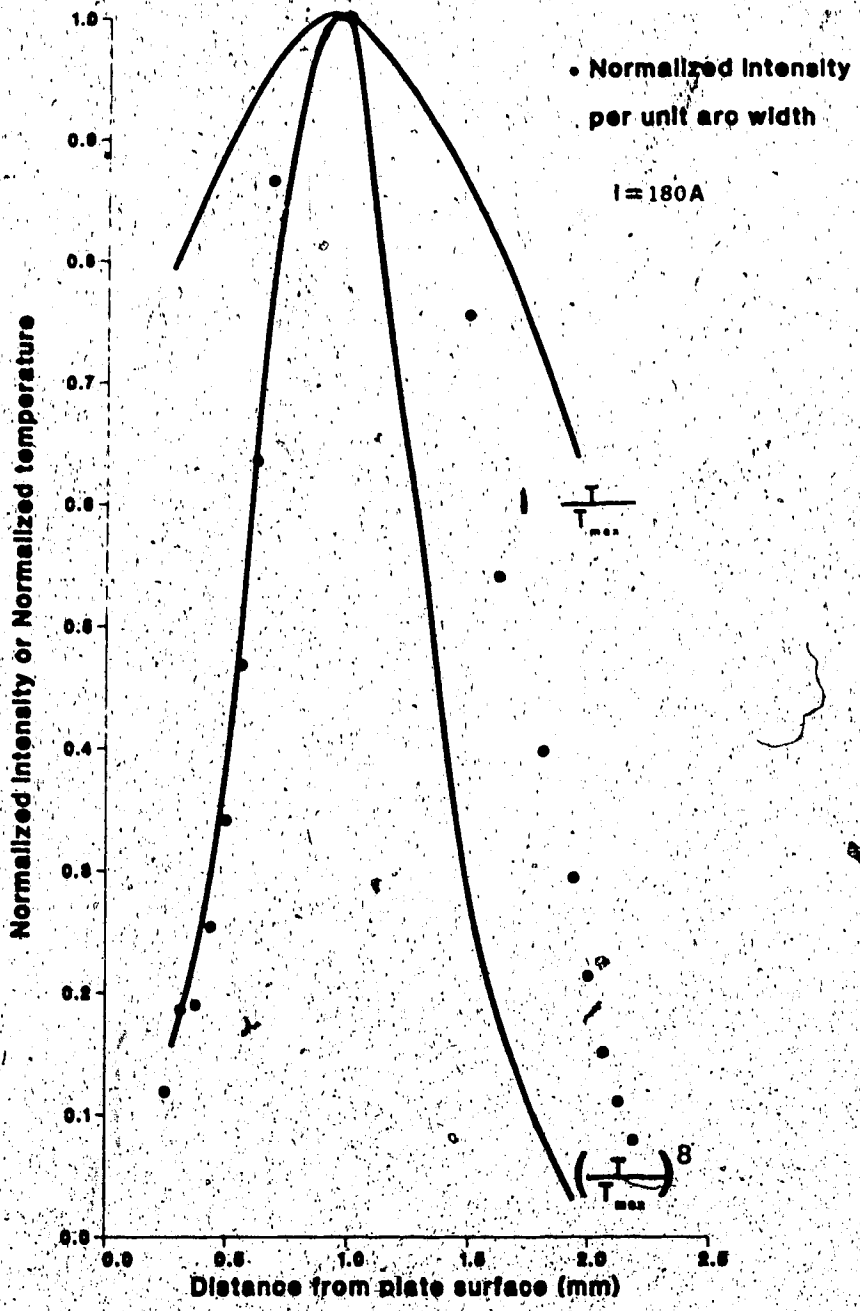

Figure 5.11 Spatial variation of normalized intensity per unit arc width for a current of 180 A.

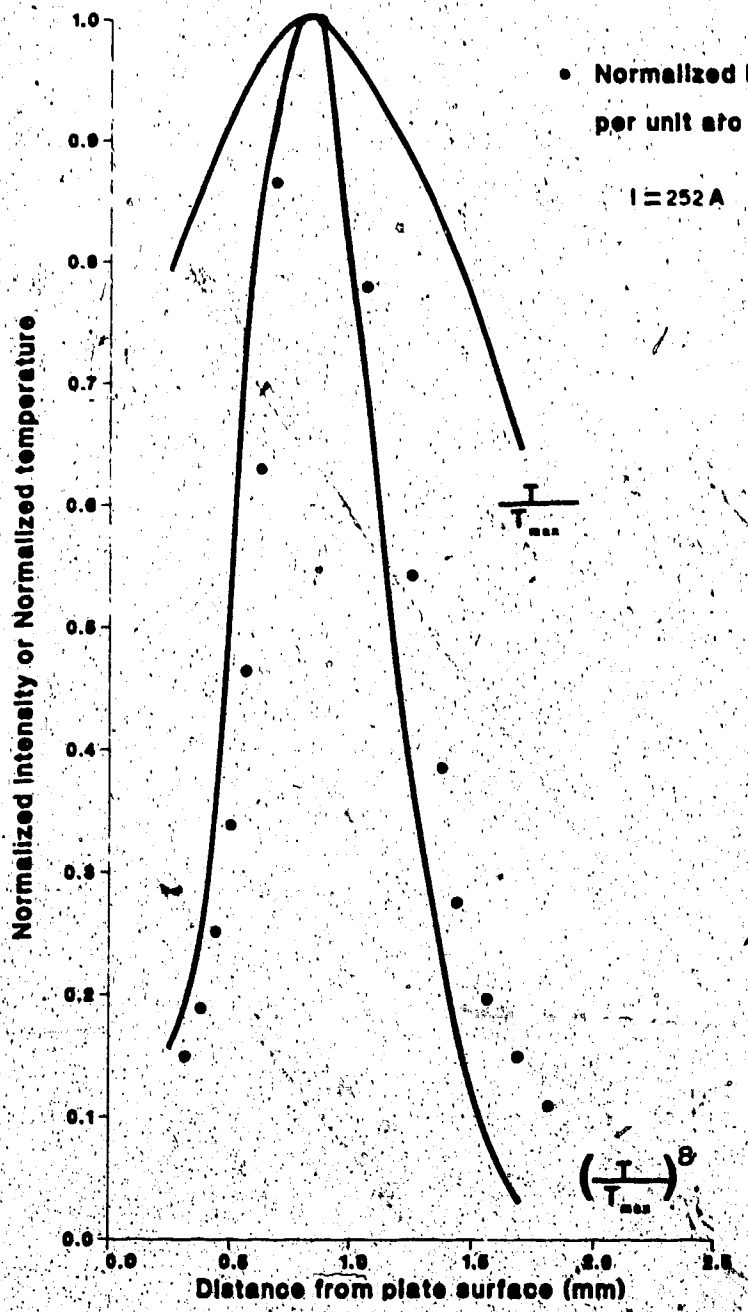

Figure 5.12 Spatial variation of normalized intensity per unit arc width for a current of 252 A.

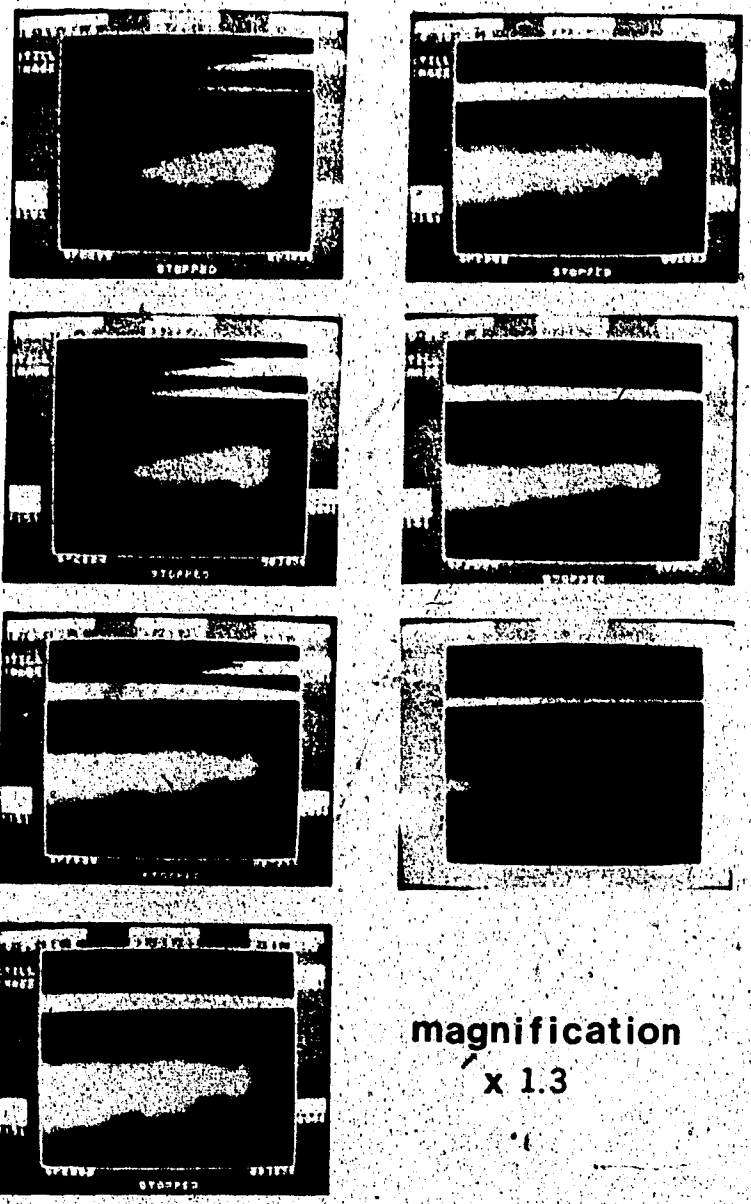

Plate 5.9 Framing pictures of an arc within a 4 mm double wedge gap at an initial charging voltage of 1 kV, series resistance of 1/6 Ω and an air flow speed of 480 m/s.

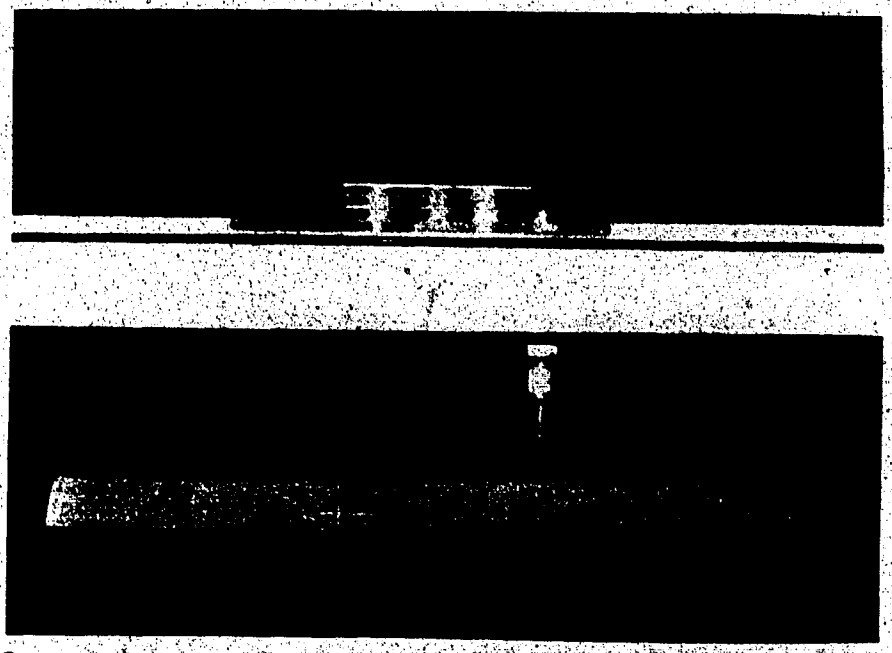

Plate 5.10 Set-up of the bottom half multiple plate stacks.

set at 1000 V or 1500 V for the initial voltage across the electrodes, $\frac{1}{6}$ Ω for the series resistance and 480 m/s for the air flow speed.

Plate 5.11 illustrates the physical and electrical characteristics of the arc within the stack for an electrode gap separation of 6 mm. The arc voltage stayed at a fairly steady value of 200 V for a current ranging from 300 A to 0 A. The framing pictures reveal that the arc only penetrated a short distance into the double plate slot. However, the arc width increased quite significantly. Plate 5.12 shows that the arc filled the various gaps of the stack for an electrode gap width of 2.2 cm. In this case, the arc width could not be measured due to the superposition of various arc sections when it is viewed in a direction perpendicular to the plate. The arc voltage characteristic shows that the magnitude varied from 500 to 1500 V as its current magnitude dropped steadily from 380 A to 0 A after the shock arrived.

5.4.7 Arc temperature profile

The temperature of the boundary layered arc can be estimated by matching the peaks of the normalized luminosity profile and the temperature profile shown in Figure 4.7. The temperature peak is located at a normalized distance derived

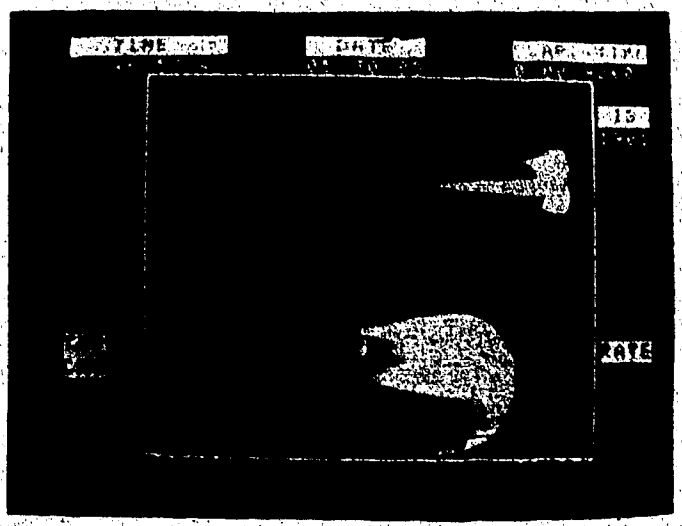

Electrode gap width : 6 mm

f-stop : f/8

Taken at 2.5 ms after shock entered the gap

(a)

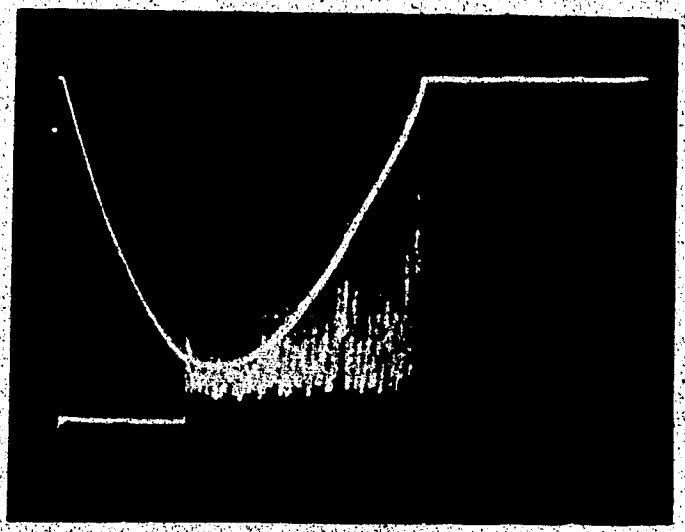

Arc charging voltage : 1 kV

Arc current : 60 A/div

Arc voltage : 200 V/div

1 ms/div

(b)

Plate 5.11 Arc pattern, arc current and arc voltage characteristics at an electrode gap width of 6 mm.

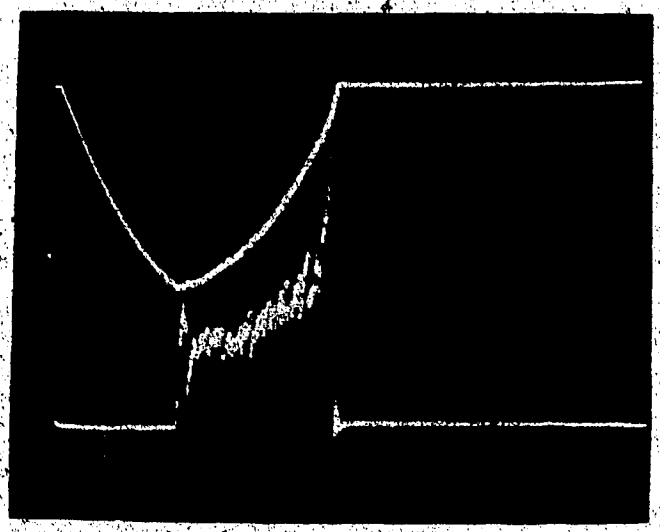

Arc charging voltage : 1.5 kV

Arc current : 120 A/div

Arc voltage : 500 V/div

1 ms/div

(a)

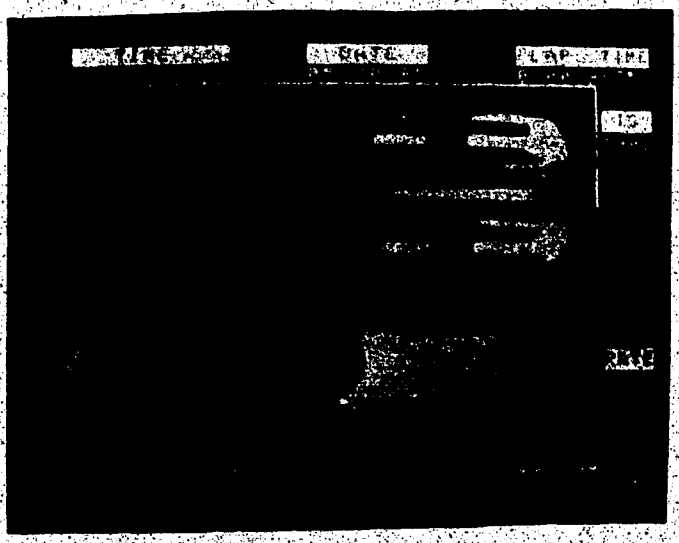

Side view of arc

f-stop : f/11

Neutral density filter : 2%

Taken at 0.5 ms after the arc entered the gap

(b)

Plate 5.12 Arc pattern, arc current and arc voltage at an electrode gap separation of 2.2 cm.

from Equation 4.21 as :

$$\eta_A \left[\frac{T_0}{T_{max}}\right] = y\left[\frac{U_0}{\nu_0 x}\right]^{1/2} \left[\frac{T_0}{T_{max}}\right] = 1.7 \qquad (5.26)$$

By matching this normalized distance to the distance of the luminosity peak y_{max} from the plate surface, the maximum arc core temperature was found to vary between 24 and 27 times the ambient temperature for currents ranging between 90 and 250 A.

The actual spatial spread, y , of the temperature profile can also be obtained by denormalizing the value of $y\left[\frac{U_0}{\nu_0 x}\right]^{1/2} \left[\frac{T_0}{T_{max}}\right]$ with the known $\frac{T_{max}}{T_0}$. The temperature profiles for the various current magnitudes are shown in Figure 5.9 to 5.12. To relate the luminosity profile to these denormalized temperature profiles, we use a simple luminosity $\propto$ (temperature)^8 power law relationship derived from data given by Schreiber [32]. The measured intensity was found to have a better match on the side near to the plate. The matching demonstrated that the arc behaved as what was predicted by the one dimensional theory. However, on the other side of the intensity profile, the arc intensity does not follow closely the $\left[\frac{T}{T_{max}}\right]^8$ relationship, but somewhat lower power of T. This is possibly due to the presence of convection in addition to conduction. The arc is thus cooler than what is predicted.

5.4.8 Aspect ratio of the arc

Streak and framing pictures of the arc revealed that the arc expanded parallel to the plate surface and perpendicular to the flows. With the photodensitometric analysis, both the arc width and thickness were found to be in a ratio of 3:1 for current magnitudes ranging between 96 A and 250 A as shown in Table 6.1.

Total current (A)	Width (mm)	Thickness (mm)	Aspect ratio
36	5.2	2.7	2
96	9.2	3.0	3
160	9.0	3.2	3
180	8.2	2.7	3
250	8.2	2.5	3

Table 6.1 Aspect ratios for arc at various currents

Such a departure from one dimensional behaviour is a likely result of the onset of nozzle clogging and will in fact do much to ameliorate that effect.

5.5 Discussion

Electrical measurements of the arc within a double plate system were taken with various combinations of arc voltages, arc currents, flow velocity, wedge slot width and electrode gap width. For both double plate and multiple plate systems, the arc was observed to form either an 'in and out' arc or a single layered arc within the channel. Plates 5.5, 5.6, 5.11(a) and 5.12(b) show that the arc boundary layers joined downstream within the gap. Experimental results indicated in Figure 5.2 that the arc followed closely the predicted field-current characteristic for the 'in and out' and the unidirectional current cases.

The densitometric scanning of the streak photographs suggests a method of finding the physical dimensions of an electric arc by means of its own luminosity. A matching of the luminosity and the temperature peaks given in Figure 4.7 enabled the computation of the arc core temperature. It was found to be 24 to 27 times the room temperature. The luminosity profile is related to the temperature profile through a relationship of luminosity being proportional to $(\text{temperature})^8$. They were found to match closely near the surface plate. However, the predicted temperatures farther away from the plate are less than the temperature indicated by the arc intensity.

The experimental field current data for the unidirectional current case were also used to compare with the theoretical one dimensional theory given in Chapter Four. Satisfactory agreement between theory and experiment is shown in Figure 5.13 for current magnitudes ranging from 96 A to 252 A. Such good agreement suggests that in unidirectional current case, the arc formed a boundary layer which was about the same thickness as the hydrodynamic boundary layer when expanded by temperature increase.

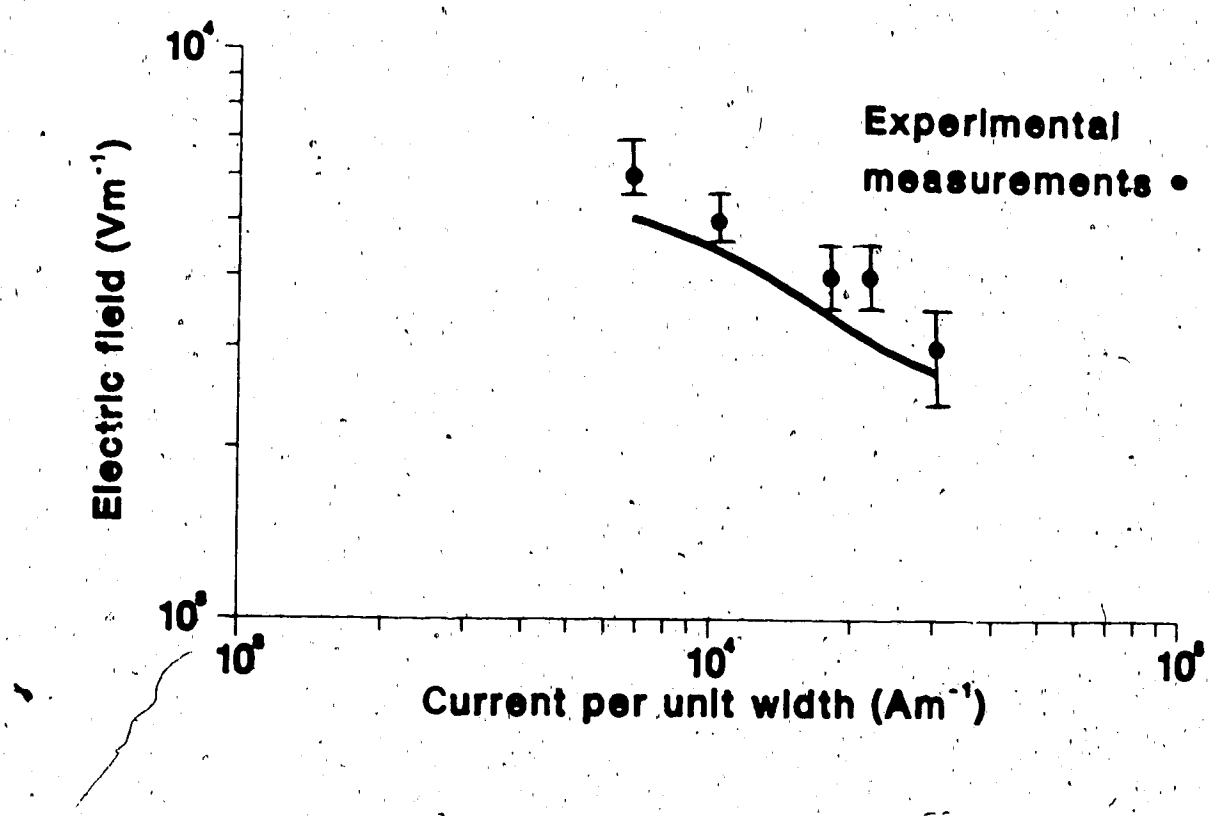

Figure 5.13 Electric field variation with current per unit width for a unidirectional arc.

6. Conclusion

The properties of an electric arc flowing along a flat surface have been investigated. Theoretical models for arcs flowing on a single flat surface interacting with a double plate gap and a multiple stack of plates were derived. Experimental measurements of axial electric field, arc current and arc thickness were found to be in reasonable agreement with the calculated values. The various cases of study are summarized in the following sections.

6.1 Single plate system

The Prandtl boundary layer equations were solved with the inclusion of a temperature transformation. Arc temperature profiles and the electric field current relationship were derived with the assumption of a two dimensional laminar flow situation and simplifications of the temperature variations of viscosity, specific heat, thermal conductivity, electrical conductivity and density. Experimental data revealed that the arc was not 'cut' by the edge as described by Prince. Instead, the arc formed a boundary layer along the plate surface as predicted by the theory. The arc thickness was derived to be of the order of a few hydrodynamic boundary layers and was measured to be within 2 mm at a downstream distance of 1.5 cm from the

leading edge and the electric field was within 5 x 10^3 V/m for various current magnitudes. Although the model is based on a two dimensional flow situation, the predicted field current characteristic reasonably agrees with the measured data discussed in Chapter 4.

6.2 Double plate system

In this situation, the arc is forced to flow between two plates so that it is limited in its ability to expand in the direction perpendicular to the flat surface. The arc flow can fall into three different configurations upon entering the gap between two plates : (1) at low flow speed, the arc initially flows as two separate boundary layers along the inner surfaces of the plate. Eventually, the two layers join together as they stretch and expand downstream (see Plate 5.5 and 5.6). The arc current flows in both directions relative to the gas flow direction; (2) at high flow speed, the arc extends beyond the plate length so that it joins with other parts of the arc. As a result, a single layered arc flows along the channel. The arc current is in the same direction of the gas flow; (3) when the double plate gap is reduced to less than a critical width, the flow speed within the gap increases if the same mass flow is maintained. The rate of cooling is hence increased. However,

an arc will tend to retain its energy. As a result, the arc will not penetrate into the gap. Analytical models for the three configurations were derived with Equations 5.1, 5.6 and 5.20. The derived field current characteristics, as shown in Figure 5.2, were compared with the measurements. Agreement for cases (1) and (2) was within 45% and 7% respectively.

6.3 Multiple plate system

A multiple plate system provides a more realistic study of the arc quenching mechanism in an arc chute. The plate array serves as a heatsink for the arc and causes enough heat lost to stop the arc from penetrating into the channels. In fact, the array creates a clogging problem for the arc which will be discussed in the next section. Framing pictures in Figure 5.11(a) and Figure 5.12(b) indicate that the arc could only penetrate a short distance into the gaps. Moreover, the arc followed the behaviour of either the 'in and out' or the unidirectional current loops. The available experimental field current characteristic was found to be in agreement within a maximum error of 17% for the unidirectional current case as shown in Figure 5.2 (case 2).

6.4 Variation of arc characteristics over the complete spectrum of flow velocities

For situations where the current flow is unidirectional, either on one side of a single plate or within a confined channel, the appropriate calculations described should be reasonably realistic since in the first case the velocity field will be close to that assumed in the model and in the second case it does not influence the electric field-current characteristics in question.

For the other multiple plate interactions, the assumptions of a constant free stream velocity poses substantial difficulties - Choking or 'nozzle clogging'.

Initially, at low flow velocity, the ratio $E_\perp/u_0$ will hold constant along the curve (case 3) in Figure 5.2. As the velocity increases, the thickness of the arc eventually becomes less than the plate separation 2D, i.e. when (Figure 5.5):

$$2D\left[\frac{u_0 \rho_0 C_{p0}}{K_0}\right]\left[\frac{T_0}{T}\right] \simeq 1$$

which with $\frac{T_0}{T} \simeq 10^{-1}$, and the Prandtl Number $\frac{\nu_0 C_{p0} \rho_0}{K_0} \simeq 0.3$ is [27] equivalent to :

$$R_D \simeq 10^1 \text{ ---> } 10^2 \qquad (6.1)$$

At this point, it is clear that the planar 'heatsink' property of the array is no longer viable and that the arc will quite naturally intrude into the channel downstream to assume the boundary layer configuration of case 1. Thus, the dividing line between case 3 and case 1 behaviour can be set at the level given by Equation 6.1.

In practice, the matter of whether the arc forms at the entrance of a channel or enters the channel may well be governed by the one dimensional version of the phenomenon of 'nozzle clogging' [33]. Since the arc and hydrodynamic boundary layers are of similar thickness, the condition that the arc boundary layers meet somewhere along the length L of the channel (case 1) implies that the hydrodynamic boundary layers also meet, or are at least close to this condition. Under these circumstances, we can expect that the bulk flow velocity through the channel will be significantly reduced below its upstream value (i.e. u_0 in Figure 5.2 will be reduced). Both arc and hydrodynamic boundary layers are expanded in thickness by a factor $\simeq \frac{T_{max}}{T_0}$ above the room temperature values and it is this phenomenon of an arc heated and expanded hydrodynamic boundary layer which significantly reduces the bulk flow velocity below its value when no arc is present, that is known as 'nozzle clogging'. From Equation 5.1, we see that the boundary layers will meet

when

$$D\left[\frac{u_0}{\nu_0 x}\right]\left[\frac{T_0}{T_{max}}\right]^{1/2} \simeq 2$$

which using the same approximations as for the case 3/case 1 dividing line gives :

$$R_D(\frac{D}{L}) \simeq 10^3 \qquad (6.2)$$

This value of $R_D(\frac{D}{L})$ will likely define the boundary line between the 'in and out' current loop (case 1) and unidirectional current (case 2) behaviour, since at higher values of $R_D(\frac{D}{L})$ the two boundary layer currents will not close within the channel.

The onset of choking within the channel at values of $R_D(\frac{D}{L})$ between 10^1 and 10^3 does of course imply a reduction in the free stream velocity within the channel. This has two results: first it throws the results of the case 1 theory into doubt - at least at the lower end of the range of $R_D(\frac{D}{L})$. Second, by reducing the effective value of R_D (due to retardation of flow in the channel), it could lead to case 3 behaviour occurring at higher values of R_D based on the upstream velocity than expected via Equation 6.1. Thus, the onset of case 1 behaviour as $R_D(\frac{D}{L})$ is decreased below the order of 10^3 may be followed quite closely by a transition

to case 3 behaviour.

In summary then, the onset of arc induced choking (or 'nozzle clogging') in the channel may reduce the range of applicability of the case 1 model to a quite restricted variation in the neighbourhood of $R_D(\frac{D}{L}) \simeq 10^3$ (in the experiment described here) rather than the range 10^1 and 10^3 envisaged at first.

6.5 Discussion

The investigations of different arc flow configurations lead to a better understanding of the behaviour of the arc within the arc chute. Although current magnitude and flow speed were smaller in scale than in the practical situation, the fundamental principle of boundary layer flow can still be verified.

The study of an arc flowing within a double plate system shows that the arc within the arc chute plates behaves as either two boundary layers which meet downstream or as a layered arc which fills the whole gap. The agreement between the luminosity and temperature profiles near the plate surface suggests that conduction through the plates is a major cooling mechanism. For the arc portion farther away from the plate surface, both convection and conduction take place. Results in Figure 5.9 - 5.11 show that a lower arc

temperature recorded than the one predicted by the single plate theory. The matching of the profiles implies that the presence of an additional plate on the layered arc does not significantly affect the heat transfer mechanism. If the field current relationship derived from the single plate theory (Figure 5.13) is compared to the one for the 'in and out' case and the unidirectional case (Figure 5.2(case 1 and 2)), it can be seen that the field magnitude is lower for the case derived from the single plate theory. It is believed that less cooling effect occurs in the single plate situation since a higher flow speed is achieved in the double plate system for a constant mass flow. A higher arc temperature results in the single plate system. Consequently, the electrical conductivity attains a higher value and leads to a lower electric field. This indicates that the optimum separation of the plates in the arc chute depends on the current magnitude being interrupted. The separation should be designed in such a way that the incoming arc can fill the gap so that its heat can be conducted away from the two surfaces in addition to convective losses.

Although the present work gives a physical insight of how the arc is cooled within the chute plates, there are other factors remained to be investigated. Slepian [4]

suggested that turbulent mixing constitutes the major arc quenching mechanism and it would be worthwhile to investigate into this effect. It is likely that there is considerable turbulence in the arc front due to the interference of the electrode assembly with the flow. A preliminary investigation on the turbulent effects was done (see Appendix 2). The non-penetrating phenomenon of the arc suggests that further investigation into the problem of nozzle clogging is worthwhile. It has been known that such a problem exists in the axial blast circuit breakers. Finally, three dimensional modelling will give a more appropriate and accurate account of the arc broadening phenomenon.

References

[1] RIEDER W.:'Circuit Breakers', Scientific American, pp.81, January 1971.

[2] RIEDER W.:'Circuit Breakers', IEEE Spectrum, July 1970, pp.35-43; August 1970, pp.90-94; September 1970, pp.80-84.

[3] CASSIE A.M.:'Power System Switchgear', The Electrical Journal, April 1959, pp.991-997.

[4] SLEPIAN J.:'The Electric Arc in Circuit Interrupters', J. Franklin Institute, 1932, Vol.214, pp.413-442.

[5] GUILE A.E.:'Electric Arcs, their electrode processes and engineering applications', IEE Proc., Sept. 1984, Vol.131, PT.A., No.7, pp.450-480.

[6] COBINE J.:'Gaseous Electronics' (Dover, 1958).

[7] EDELS H.:'Properties and Theory of the Electric Arc', IEE, Feb. 1961, pp.55-69.

[8] FLURSCHEIM C.H.:'Power Circuit Breaker Theory and Design' (Peter Peregrinus, 1975).

[9] BROWNE JR. T.E.:'Circuit Interruption Theory and Techniques' (Marcel Dekker, 1984).

[10] LEE T. H. : 'Physics and Engineering of High Power Switching Devices', (MIT Press, 1975), p.380.

[11] BOEHNE E.W., LINDE L.J.:'Magne-Blast Air Circuit Breaker for 5000 Volt Service', General Electric

Review, 1939, 42, pp.401-408.

[12] REECE M.P.:'Air Break Arc Chute Circuit Breakers; Discussion of Published Information on Modern Types', The British Electrical and Allied Industries Research Association. G/XT 135, June 1952.

[13] BROWN JR. T.E.:'Circuit Interruption Theory and Techniques' (Marcel Dekker, 1984) Chapter 11, p.425.

[14] LUDWIG I.R., BAKER B.P.:'A Vertical Flow Outdoor Compressed Air Breaker', AIEE Transactions, May 1941, Vol.60, pp.217-222.

[15] BENNETT R.M., Wyman B.W.:'Medium Capacity Air Blast Circuit Breakers for Metal Clad Switchgear', AIEE Transactions, 1941, Vol.60, pp.383-388.

[16] STRANG H.E., BOISSEAU A.C.:'Design and Construction of High Capacity Air Blast Circuit Breakers', AIEE Transactions, 1940, Vol.59, pp.522-527.

[17] PRINCE D.C., HENLEY J.A., RANKIN W.K.:'The Cross Air Blast Circuit Breaker', AIEE Transactions, 1940, Vol.59, pp.510-517.

[18] SLEPIAN J.:'Displacement and Diffusion in Fluid Flow Arc Extinction', AIEE Transactions, April 1941, Vol.60, pp.162-167.

[19] SMY P.R., TOPHAM D.:'Boundary Layer Cooling of Atmospheric Arcs', 1978, 5th Int., Conf. on Gas

Discharges, Liverpool, IEE Conference Publication, 124.

[20] WOODS H.A., SMY P.R.:'The Arc Supported Boundary Layer', 1980, 6th Int., Conf. on Gas Discharges, Liverpool, IEE Conference Publication, 189, p.75.

[21] LEE T.H.:'Physics and Engineering of High Power Switching Devices' (MIT press, 1975).

[22] LUDWIG L.R., RAWLINS R.S. and BAKER B.P.:'A New 15 kV Pneumatic circuit interrupter', Electrical Engineer, 1940, Vol.59, pp.528-533.

[23] SELZER A.:'Switching in Vacuum; A Review', IEEE Spectrum, June, 1971, pp.26-37.

[24] SIMEONI D., Ph.D. Thesis, University of Alberta, 1985.

[25] HALEY R., M.Sc. Thesis, University of Alberta, 1986.

[26] WELLS A.:'Numerical Calculations of the Properties of Axially Symmetric Arc Columns', R.A.E. Tech. Report, No. 67076, 1967.

[27] AU S., SANTIAGO J., SMY P.R.:'Analysis of the arc formed along the surface of a flat plate immersed in a lamina flow of gas', IEE Proc., November, 1984, Nov. 131, Pt. A, No. 8, pp.605-609.

[28] YUAN S.W.:'Foundations of Fluid Mechanics' (Prentice-Hall, 1967) p.312.

[29] SCHLICHTING H. : 'Boundary Layer Theory', (McGraw-Hill, 7th edition, 1979), p.340.

[30] NIEMEYER L.:'Evaporation dominated high current arcs in narrow channels', IEEE Trans., 1978, PAS-97, pp.950-958.

[31] TOPHAM D.R.:'The electric arc in constant pressure axial gas flow', J. Phys. D., 1971, 4, pp.1114-1125.

[32] P.W.SCHREIBER, A.M.HUNTER, K.R.BENEDETTO, 'Electrical conductivity and total radiant power of air plasma', 2nd Int., Conf. on Gas Discharges and their Applications, 1972, IEE Conference Publication, 90, p.361.

[33] L.C.Campbell, J.L.Dallachy : 'Effects of Nozzle Clogging on Air and SF_6 blasted arc', 5th Inter. Conf. on Gas Discharges, 11-14 September, 1978, IEE Conference Publication, 165, 1978, p.43-46.

[34] BRADLEY J.N.:'Shock Waves in Chemistry and Physics' (John Wiley & Sons, 1962), pp. 47 - 48.

[35] HINZE J. O. : 'Turbulence - An Introduction to Its Mechanism and Theory', (McGraw - Hill, 1959), p.216.

7. Appendix 1

The speed of gas flow behind a shock wave is calculated according to the equations given by Bradley [34]. For the purpose of convenience, the equations are given below:

$$u_2 = f(p_2) = a_1\left[\frac{p_2}{p_1} - 1\right]\sqrt{\frac{2}{\gamma_1\left[(\gamma_1+1)\frac{p_2}{p_1} + (\gamma_1 - 1)\right]}} \tag{A.1}$$

$$\frac{p_4}{p_1} = \frac{p_2}{p_1}\left[1 - \frac{a_1}{a_4}(\gamma_4 - 1)\sqrt{\frac{\frac{p_2}{p_1} - 1}{2\gamma_1\left[(\gamma_1+1)\frac{p_2}{p_1} + (\gamma_1 - 1)\right]}}\right]^{\frac{-2\gamma_4}{\gamma_4 - 1}} \tag{A.2}$$

u_2 -- flow speed behind the shock

γ_1 -- ratio of specific heat in the driven section

γ_4 -- ratio of specific heat in the driver section

a_1 -- sound speed in the driven section

a_4 -- sound speed in the driver section

p_1 -- pressure in the driven section

p_2 -- pressure behind the shock

p_4 -- pressure in the driver section

8. Appendix 2

The electrical behaviour and flow pattern of an arc layer under the influence of turbulent air flow were studied by mounting a rectangular grid in the midst of the air flowing within a shock tube. A 3.0 cm x 6.0 cm ($1\frac{1}{4}$" x $2\frac{1}{4}$") rectangular grid with 1.5 mm ($\frac{1}{16}$") diameter tungsten rods forming meshes of size 1.5 cm x 1.0 cm ($\frac{9}{16}$" x $\frac{5}{16}$") was mounted about 20 cm (8") in front of a double plate gap of 4 mm apart, as shown in Figure 8.1.

An electric arc was discharged at 1 KV through a $\frac{1}{6}$ Ω shunt resistor and was blown by air flowing at a speed of 480 m/s. Both width and thickness of the arc profile were recorded with the SP2000 camera. The electric field and current were recorded simultaneously. Plate 8.1 shows the field current characteristic for an arc discharged at 1 KV through a $\frac{1}{6}$ Ω shunt resistor. The electric field magnitude varies from 25 V/cm to 120 V/cm for a current range of 300 A. The thickness of the profile shown in plate 8.2 appears to increase parabolically downstream and was measured to be about 2 mm. The created turbulence apparently did not affect the thickness of the arc profile significantly.

The mesh size was reduced by replacing the 1.5 mm ($\frac{1}{16}$") diameter rods with 3 mm diameter tungsten rods. However, the

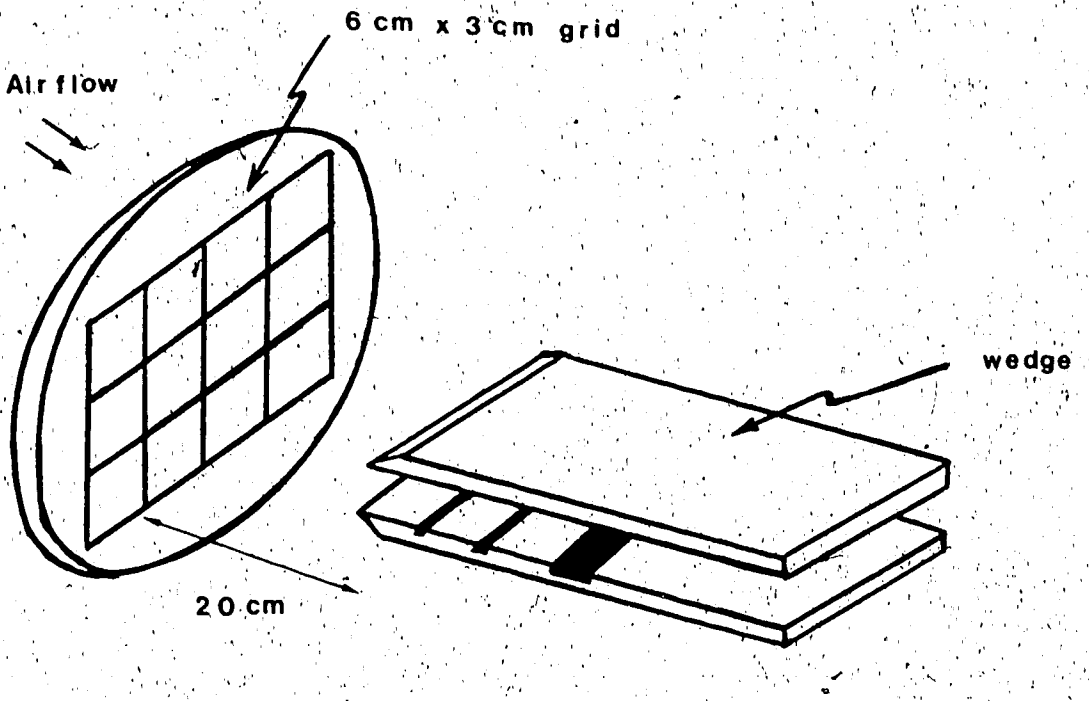

Figure 8.1 Schematic of grid and double wedge arrangement.

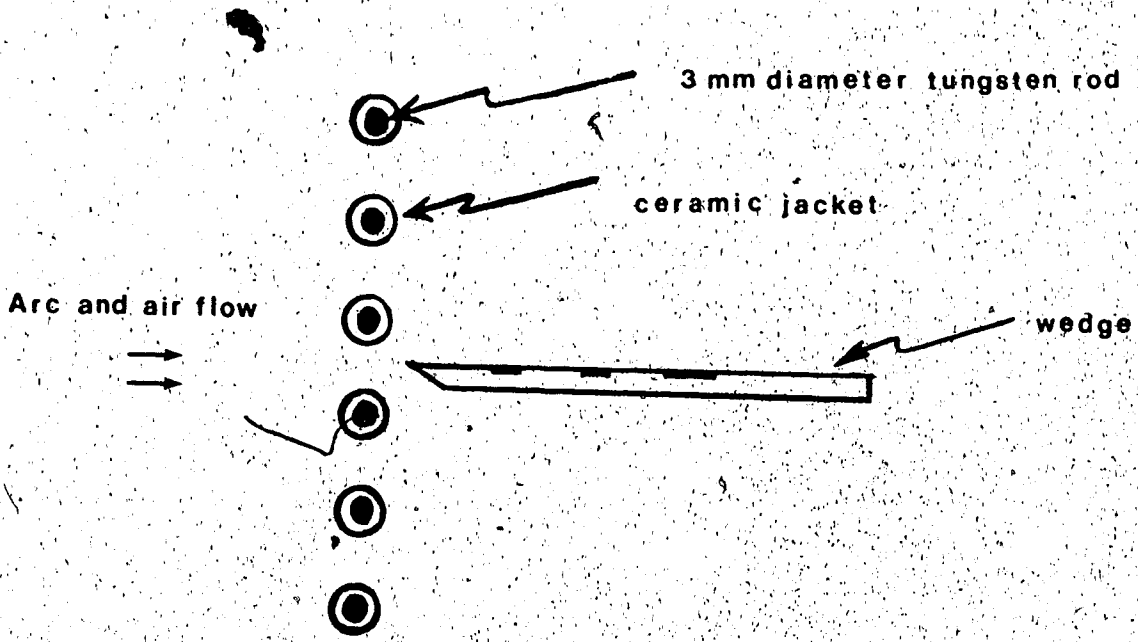

Figure 8.2 Schematic of a pile of rods and wedge arrangement.

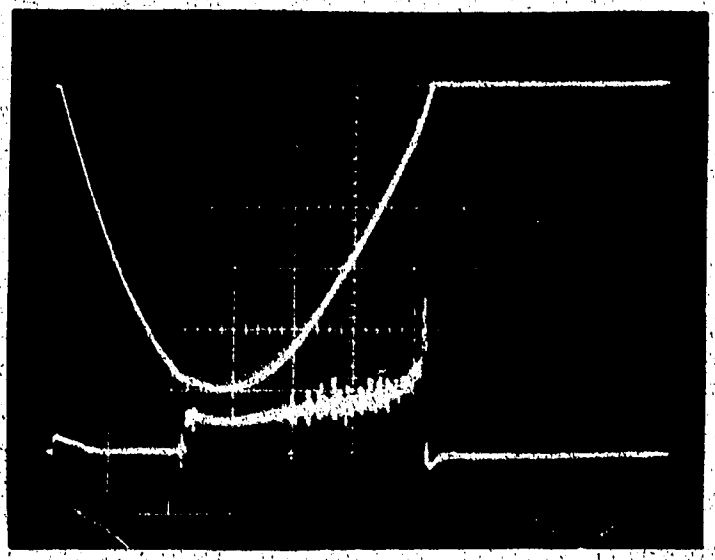

Arc current : 60 A/div

Arc charging voltage : 1 kv

Flow speed : 480 m/sec

Differential voltage between probes at 1 cm apart : 50 v/div

1 ms/div

Plate 8.1 Electrical characteristics of an arc under turbulent air flow.

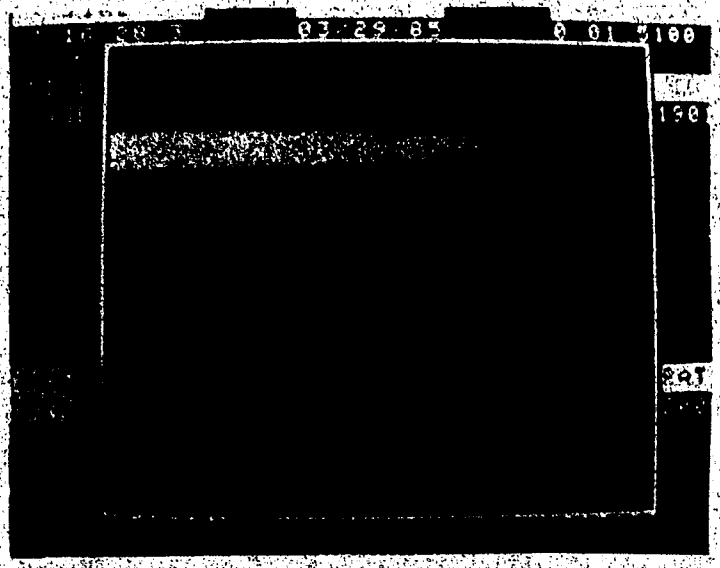

Magnification : x 3

Plate 8.2 Thickness and width of arc profile corresponding to Plate 8.1.

thickness of the arc layer profile appeared to remain unchanged and was measured to be about 1.5 mm to 2.0 mm.

A pile of 3 mm ($\frac{1}{8}$") diameter steel rods insulated with ceramic jackets were placed in front of the wedge. The rods were arranged in a pile perpendicular to the surface of the wedge. Each rod was spaced 4.5 mm ($\frac{3}{16}$") from another rod. One of the rods was arranged to be fairly close in height to the leading edge of the lower wedge plate (Figure 8.2). An electric arc was produced by discharging 1 KV through a $\frac{1}{6}$ Ω shunt resistor. Air flow speed was maintained at 480 m/s. The profile of the arc is shown in Plate 8.3. The thickness of the profile appears not expanding parabolically but oscillating downstream. It maintains a thickness of approximately 2 mm. The electric field magnitude shown in Plate 8.4 decreases. It varies from 8 V/cm to 90 V/cm for a current range of 300 A.

The turbulence introduced by means of a rectangular grid did not significantly affect the physical and electrical properties of the arc. According to the measurements by Batchelor and Townsend [35], the turbulence intensity at a distance of 20 times the mesh size is estimated to be 3 %. Moreover, the turbulence intensity decreases linearly with distances beyond the described criterion. The present arrangement had the grid situated at

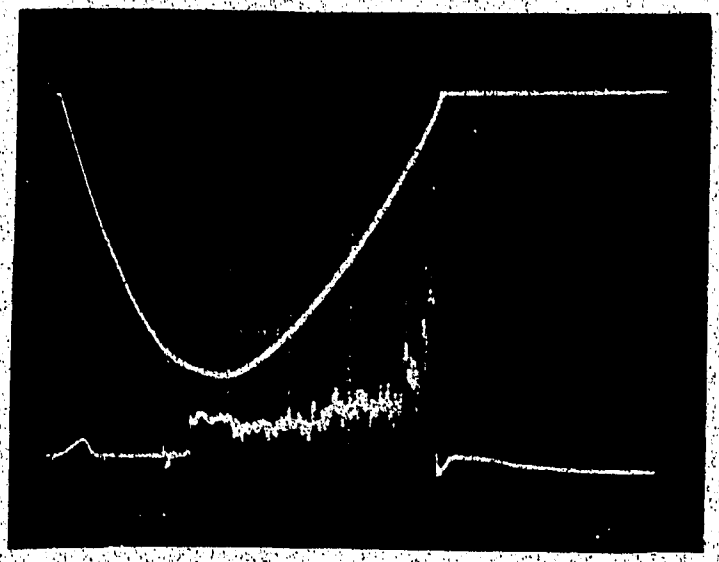

Arc current : 60 A/div

Arc charging voltage : 1 kv

Flow speed : 480 m/sec

Differential voltage between probes at 1 cm apart : 50 v/div

1 ms/div

Plate 8.3 Thickness and width of an arc profile created behind a pile of rods.

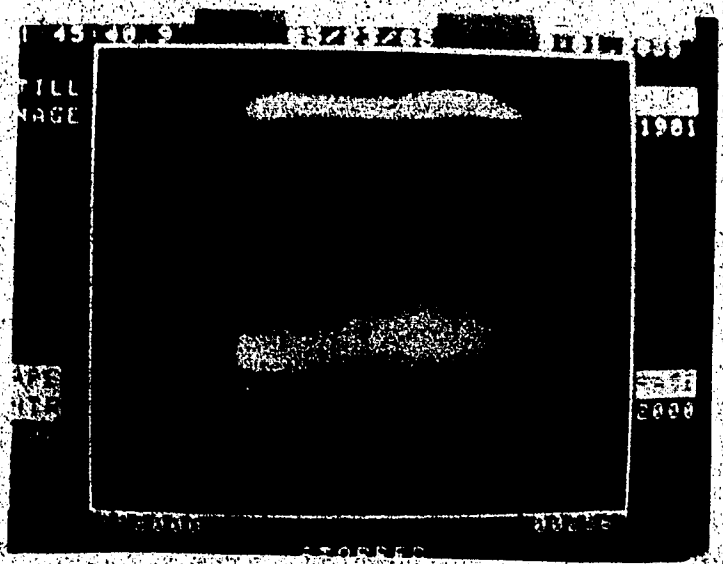

Magnification : x 1.5

Plate 8.4 Electric characteristic corresponding to the arc profile shown in Plate 8.3.

a distance of 20 times the mesh size. Hence, the effect of turbulence is small in this case.

In the second case, the arc was forced through a pile of rods placed next to the leading edge of the wedge. Drastic changes in the flow condition resulted an oscillatory electric arc boundary profile as shown in Plate 8.3. It may be concluded that turbulence contributed a significant effect in this situation. However, further investigations are needed in order to come up with satisfactory conclusions.